2017

Formulation and testing of biodegradable polymeric coating on zinc wires in cardiovascular stent application

Avishan Arab Shomali
Michigan Technological University, aarabsho@mtu.edu

FORMULATION AND TESTING OF BIODEGRADABLE POLYMERIC COATING ON ZINC WIRES IN CARDIOVASCULAR STENT APPLICATION

By

Avishan Arab Shomali

A THESIS

Submitted in partial fulfillment of the requirements for the degree of

MASTER OF SCIENCE

In Materials Science and Engineering

MICHIGAN TECHNOLOGICAL UNIVERSITY

2017

This thesis has been approved in partial fulfillment of the requirements for the Degree of MASTER OF SCIENCE in Materials Science and Engineering.

Department of Materials Science and Engineering

Thesis Advisor: *Jaroslaw W. Drelich, Ph.D.*

Committee Member: *Jeremy Goldman, Ph.D.*

Committee Member: *Daniel Seguin, Ph.D.*

Department Chair: *Stephen L. Kampe, Ph.D.*

Table of Contents

List of Figures

List of Tables

Acknowledgments

I would like to express my gratitude to my advisor Dr. Jaroslaw Drelich for his support, insight, and guidance. It has truly been a pleasure working on this project with you.

I would also like to thank Dr. Goldman, Dr. Seguin, and Dr. Hackney for their diligent work throughout the research project.

Finally, I would like to thank my parents for their love and support.

1 Abstract

Biodegradable and biocompatible poly (L-lactic-acid) (PLLA) coating was applied on a modified zinc (Zn) substrate by dip coating, with the intent to delay the bio-corrosion and slow the degradation rate of zinc substrate. 3-(Trimethoxysilyl) propyl methacrylate (MPS) was used for modification of the zinc substrate for promoting the adhesion between the metallic substrate and the polymer coating. It is hypothesized that the delay in Zn biodegradation could be useful in the first several weeks to prevent the early loss of mechanical integrity of the endovascular stent and to improve the healing process of the diseased vascular site. The PLLA coating was used in this study because of its biodegradability, favorable degradation rate, hydrophobicity and favorable mechanical properties. Static immersion, electrochemical and inductively coupled plasma (ICP) tests were used to investigate the degradation behavior of a polymer coated modified Zn substrate. Two uniform polymer layers with thickness of 1 and 3 μm were coated on the Zn substrate. The potentiodynamic polarization test indicated that the 1 μm polymer coated specimen has higher corrosion potentials (E_{corr}) and lower corrosion cur rents (i_{corr}) in the simulated body fluid (SBF) compared to the uncoated Zn. AC impedance measurement in EIS test also demonstrated a significant improvement in the impedance and polarization resistance of the coated Zn substrate. However, after 10 days of immersion in the SBF, the impedance reduced drastically which is indicative of a coating degradation and penetration of the electrolyte to the zinc substrate. Immersion degradation studies showed that the cross-sectional area (CSA) reduction and penetration rate (PR) for polymer coated samples are 5 times smaller than for uncoated samples after 14 days of immersion in SBF solution. Results of the ICP method indicated an increase in the release of the Zn^{2+} to the solution for the uncoated Zn, while the 1 μm PLLA coated sample demonstrated much slower release rate of Zn^{2+} and the concentration of Zn ion during the 14 days' immersion in SBF was almost the same. In *in vivo* studies, the polymer-coated Zn and uncoated Zn samples were implanted into the abdominal aorta of the rats and then directed into the lumen. The explants were extracted after 0.5 to 6 months. The results of *in vivo* study indicated that the uncoated samples have approximately two times higher CSA reduction and PR in comparison to the coated samples during first 4.5 months. After 4.5 months, the CSA

reduction and PR increased significantly. However, the histological analysis of the biological tissue surrounding samples showed a reduction in biocompatibility of the polymer coated samples indicated by increasing cell toxicity and neointimal hyperplasia.

2 Introduction

Endovascular stents have become the most reliable medical devices for treating coronary artery diseases. The stents overcome the limitations and drawbacks of bypass surgery and balloon angioplasty by enabling scaffolding, widening and supporting the blocked vessel [1]. Currently, stents are made of permanent inert materials (i.e., stainless steel, cobalt-chromium alloys, titanium alloys) to remain intact in a body for a lifetime and to prevent the mechanical failure of the implanted device [2, 3]. Their major side effects include covering and encapsulation with hyperplasia tissues, chronic inflammatory reaction, and thrombogenicity [2]. In some cases, the need for second surgery to remove these permanent stents after completion of the healing process is another limitation of permanent stents [2]. The drawbacks of permanent stents drive efforts towards the development of temporary stents made from bioabsorbable materials [4]. Biodegradable stents could be absorbed and metabolized by the body after serving its mechanical purpose during deployment and in the first few months after implantation [4-6]

Over the past decade, iron and magnesium and their alloys have been investigated as the candidate materials for endovascular stent application. However, past and recent investigations on these materials have demonstrated that neither of these materials can be suitable for stent application [5, 7, 8]. In the case of iron and its alloys, the accumulation of iron corrosion products and reduction in the lumen cross-sectional area are of concerns [9]. Premature degradation of magnesium has limited the success of this metal for stent application [10]. Zinc was introduced as a new material for bioabsorbable stents in 2013 due to its favorable degradation rate and outstanding biocompatibility [11, 12].

Several possible techniques including surface treatments, metal alloying, materials processing to manipulate the microstructure, an organic coating of the surface could be employed to slow down zinc's bio-corrosion and maintain the mechanical integrity of the implant during the healing of the vessel wall. Alloying and manipulating the processing strategies may slow the degradation rate of the Zn-based implant, but are likely to affect the biocompatibility of the stents [13, 14]. Adding a biocompatible polymeric coating is

one of the most popular approaches in delaying bio-corrosion of biodegradable metals while maintaining their biocompatibility [15]. Polymeric coating can control the metal corrosion by isolating it from the corrosive environment or by suppressing dissolution of metal or corresponding cathodic reaction. Adding a polymeric coating not only can act as a corrosion barrier but also it can be loaded with drugs which can be released in controlled amounts to prevent post-surgery inflammations or restenosis [16]. In this thesis, a layer of poly (L-lactic-acid) (PLLA), commonly explored biodegradable and biocompatible polymer, is formulated on a zinc substrate with the aim of delaying its corrosion rate while maintaining its biocompatibility.

3 Background

3.1 Coronary artery disease (CAD) treatments

Cardiovascular disease remains a major cause of death in the United States and worldwide; 30 percent of deaths in 2009 in the United States were caused by cardiovascular disease [17, 18]. CAD develops when the arteries that supply blood to heart muscle narrowed due to the accumulation of fatty deposits, called plaque, on the inner walls of the artery [19]. Over time, as more and more plaque deposits on the artery wall, the flow of blood to the heart muscle becomes more restricted. Inadequate blood supply causes a shortening of breath and chest pain, and in the most severe cases, a heart attack may occur. Three treatments used for coronary heart disease are coronary artery bypass graft (CABG) surgery, balloon angioplasty and stenting [20-22]. In CABG surgery the blocked or narrowed portion of the artery is bypassed with a healthy blood vessel taken from another vain location. The bypass creates a new path for the blood to flow without any obstruction to the heart muscle [23]. In the balloon angioplasty, a balloon tip catheter, having a shape of a long thin tube, is inserted through an artery in the groin or wrist. Then the balloon is inflated at the site of the diseased artery with reduced diameter. The artery is widened due to the compression of the plaques against the artery wall [24, 25]. Angioplasty is also called percutaneous transluminal coronary angioplasty (PTCA).

Each of techniques for treating the coronary artery disease has its own benefits and risks. Since bypass surgery is an open heart procedure, there is a risk that the heart might stop beating during the surgery [26]. Going into general anesthesia, heart rhythm problems, blood clots, bleeding from the site of attached graft and other complications are the other drawbacks of bypass surgery [26]. Nevertheless, this technique can be more beneficial in the case of serious cardiovascular diseases [27]. Since balloon angioplasty is a less invasive surgery, it does not have many complications and risks of the bypass surgery. The re-narrowing of the artery, which is called restenosis, can occur within three to six months [28, 29]. Restenosis is a major drawback to balloon angioplasty because 25 to 60% of the patients experience it after surgery and then need to undergo the second revascularization interventions [20, 30].

Stenting is a technique which has been developed to prevent occlusion and restenosis. Stents, which are mesh-like expandable tubes were introduced in the 1980s by Sigwart *et al.* [31] to complement or replace balloon angioplasty and decrease the rate of restenosis. The first FDA approved stent was produced by Johnson and Johnson Inc. in 1994 [32].

A stent is placed around a deflated balloon catheter and then deployed into the blocked artery with a balloon catheter under x-ray visualization. Inflation of the balloon expands the stent and locks it intended destination [23]. Once the stent is deployed, the balloon is deflated and removed by the catheter. The deployed stent remains in the artery and provides scaffolding for keeping the artery open. The recoil of the artery is prevented by the expanded stent.

Efforts have been continuously put into stent research for developing new designs and materials in an attempt to improve the performance of these medical devices and to address the post-angioplasty surgery issue. Mechanical, chemical, and the extent of biocompatibility of the material used in the stent design (length and diameter of the stent, shape and thickness of the struts) are the most important factors which should be taken into consideration for designing the stent [33].

Corrosion is of paramount importance and concern because degradation of the implanted stent causes structural failure and the loss of mechanical integrity and support, which can lead to premature malfunctioning of the implant [34]. The sudden release of metallic ions into tissue surrounding the implant is another concern, particularly with rapid bio-corrosion rates [35]. Therefore, selecting the proper material in terms of its susceptibility to corrosion is of great significance. The first generation of stents were made from inert materials which resisted corrosion, such as medical grade stainless steel, Ti alloys and cobalt-chromium alloys [2]. Several complications and problems of using corrosion resistant metals, including foreign body response, chronic inflammation, late stent thrombosis, tissue loss and painful second removal surgery limits their application in vascular stents [5, 36]. Long-term implementation causes the release of toxic ions and particles, which can become a source of infection and obstruction for secondary treatments including bypass surgery [5, 37]. In order to overcome the mentioned problems a new generation stents made of bioabsorbable/biodegradable materials has been proposed [4]. For the purpose of material selection for the bioabsorbable stent, it is necessary to select a material which is both biodegradable and biocompatible and has the appropriate physical and mechanical properties for the proper functioning [4-6, 38].

3.2 Bioabsorbable stent materials

Although encouraging results have recently been reported, the new generation of bioabsorbable stents is still largely under development. The two primary stent material candidates have historically been iron (Fe) and magnesium (Mg). Iron is not a suitable material for bioabsorbable stents since its corrosion products are voluminous, are not integrated into the cellular layer, and might remain in the body for long periods [9]. As a consequence, the cross-sectional area of the lumen might also be reduced because of the accumulation of the corrosion products. The long degradation rate is another disadvantage of iron for bioabsorbable stent application. Magnesium, on the other hand, degrades less harmfully. However, magnesium and magnesium alloys demonstrate relatively fast degradation rates and low ductility which restrict them from applications as suitable biodegradable stent materials [10]. Several biocompatible alloying elements such as Ca,

Zn, Sn, Zr, Si, W, Li, C, Al, and rare earth elements (Y and Gd) have been investigated to control biodegradation and mechanical properties of Mg and Fe, and enhance their functionality and biocompatibility for vascular stent and orthopedic applications [10, 39, 40]. Different processing strategies and various mechanical, chemical and electrochemical surface treatments were also investigated to minimize the corrosion of Mg and Mg-base alloys [39, 41-43]. Although alloying and improvements in processing methodologies slower degradation rates, they introduce a possibility of reduced biocompatibility of the metal due to the formation of intermetallic phases and toxicity of the corrosion products of the alloying elements [34].

Zinc (Zn), which is one of the essential elements for basic biological functions in the body [44, 45], has been proposed recently as a suitable bioabsorbable material [11]. Its favorable and uniform degradation rate, outstanding ductility and biocompatibility make it one of the few physiologically acceptable metals for bioabsorbable stent application. It has been shown that the initial penetration rate of zinc in the body in the first 1-3 months satisfy the requirement for stent application [11, 12]. The early study with zinc also suggests that zinc degradation rate in the endovascular environment might increase after 3-4 months. Also, insufficient mechanical properties of zinc such as its low tensile strength pose limitations for its usage as a bioabsorbable stent [11]. However, its exceptional elongation to failure (60-80%) which is much higher than the requirement for stent application (15-18%) turns it to an adequate candidate for a bioabsorbable stent [11].

The main purpose of this research is to utilize surface coating to slow down the corrosion rate in the first few weeks after stent deployment, without compromising the biocompatibility of Zn stents. For this purpose, poly (L-lactide acid) (PLLA), a biodegradable and biocompatible polymer commonly used for medical implants [46, 47] is studied herein. Coatings of degradable polymers can act as a corrosion barrier and carriers for delivery drugs in order to combat in-stent neointimal formation and therefore restenosis and repeated revascularization which are the main drawbacks of PCI with bare metal stents [48]. Drug-eluting stents (DES) made of permanent stents and polymeric coatings are currently on market [16].

3.3 Polymer coating for corrosion protection and drug eluting

3.3.1 Polymer coating on permanent stents for drug delivery and/or corrosion protection

Polymeric coatings containing drugs have been applied on permanent stents to prevent restenosis and inflammation within 6 months [16]. Cypher is one of the DES which is approved by FDA [16]. Stainless steel, which is its base metal, is coated with a mixture of poly (ethylene-*co*-vinyl acetate) (PEVA) and poly (*n*butyl methacrylate) (PBMA) [16]. The mixture contains Sirolimus as the drug, which is a natural macrocyclic lactone, used to combat restenosis [16]. Also, another layer of PBMA is applied on the top of stent surface for controlling drug release [16]. The other DES which is approved by FDA is Taxus stent. Stainless steel is selected as the base metal and is coated with the mixture of poly styrene*b*- isobutylene-*b*-styrene (SIBs) with paclitaxel as the drug [16].

Another example of polymer coating on permanent materials is the Nitinol (nickel-titanium alloy) substrate coated with polyurethane [49]. The polymeric film with a thickness from 5 μm to 15 μm in this study was deposited on Nitinol coupons through a dip coating. In another experiment, brush coating was employed to increase polymer coating to 15-30 μm. The study investigated the dependence of corrosion rate of Nitinol on coating film thickness. Potentiodynamic polarization test with using Ringer's solution as the electrolyte was performed for evaluating the corrosion behavior of the samples. It was demonstrated that the corrosion rate of the uncoated samples decreased from 275 μm/year to 13 μm/year after deposition of the 30 μm polyurethane coating.

Deposition of parylene coating on the surface of the silane modified stainless steel (SS) 316L grade is another case of polymer coated permanent material for biomedical implants [50]. 20 X 20 mm^2 SS coupons with 0.8 mm thickness were first treated with a monolayer of A174 silane coupling agent by dip coating after drying the specimens with high-pressure argon at 65ºC for 30 minutes. Then parylene (poly-para-xylylene) coating was applied by chemical vapor deposition (CVD) method. EIS method was employed in order to investigate the corrosion behavior of the silane modified polymer coated SS. Two kinds of solutions were used as the electrolyte. The first solution was Hank's solution and the

second was Hank's solution with the addition of hydrogen peroxide to simulate the inflammatory response of the human body condition. Exposure of the specimens to Hank's solution for 9 days could not deteriorate the protective polymer layer and the coating was still maintaining its protective properties. However, the addition of hydrogen peroxide led to the failure of the protective layers. By analyzing the EIS plots and fitting circuit models on them it was concluded that the formed of OH- radicals attack the metal-polymer interface and lead to the deterioration of the polymer coating.

3.3.2 Polymeric coating on Mg and its alloys for corrosion protection

Magnesium and its alloys have a rapid corrosion rate. Although its high biocompatibility, favorable mechanical behavior, light weight and shock absorption making it to an outstanding element in medical application [32], its low corrosion resistance limits its widely application. Several biomedical coating has been applied on magnesium in order to improve its corrosion resistance. Anodization, metallic coating, sol-gel coating, inorganic coating and organic coating are some of the methods which have been examined for this purpose [32]. Relevant research of polymeric coating of biodegradable magnesium is briefly reviewed in the following subsections.

3.3.2.1 PLGA-Mg6Zn substrate [51]

Poly-lactic-co-glycolic acid (PLGA) was tested as a coating on the Mg6Zn substrate. Mg-based samples were dip coated with PLGA using solutions. Resulting coating thickness was approximately 33 and 72 µm. The thickness of polymeric layer could be changed by altering the concentration of PLLA in the solution. By potentiodynamic polarization test, it was demonstrated that the PLGA coatings dramatically reduced the corrosion current density (i_{Corr}) of Mg6Zn from 26.5 to 0.085 µA $cm^{-2}$for the thinner polymer coating and to 0.097 for the thicker polymer coating. The average degradation rate of the uncoated Mg6Zn sample was also compared with the coated samples by immersion test in 0.9 NaCl solution. Reduction in the degradation rate of the coated samples by at least two orders was reported. Significant improvement in the impedance of the coated samples in comparison to the bare Mg6Zn alloy was demonstrated by EIS technique. Thinner coating showed higher resistance and better performance, probably due to the existence of some defects such as

voids and flaws in the thicker polymer layer. Improvement in the cell attachment ability of polymer coated Mg6Zn substrate was also reported, in comparison to the bare metal substrate.

3.3.2.2 PLA/PCL-High Purity Mg (HPM) [52]

In other studies, a high purity magnesium was coated separately with PLA (polylactic acid) and PCL (polycaprolactone) by dip coating to the thickness of 15 and 20 μm, respectively. It was found that both PLA and PCL improved the corrosion resistance of HPM. The dynamic immersion test was used instead of the static immersion test with the aim of simulating the real circulation of blood in coronary arteries. M-SBF was also used as the test medium. Weight loss of the specimens at different time intervals was measured as an indication of the degradation rate. The weight of the specimens was increased slightly at the early stages of the experiment which can be interpreted as the absorption of water and precipitation of m-SBF. After 6 days of immersion, a significant weight loss was observed for the PLA coated sample. However, a similar decrease in weight loss occurred for the PCL coated sample after eight days. Also, the decrease was not as rapid as the PLA coated specimen. The polarization test of the coated and uncoated specimens showed that corrosion potential (E_{Corr}) of the coated specimens increased by 246 mV for the PCL-coated sample and 120 mV for the PLA-coated sample. Significant reduction in i_{corr} of the coated samples from 2.1×10^{-4} A for the uncoated HPM to 1.3×10^{-5} A for the PCL coated HPM and 3.6×10^{-5} A for PLA coated HPM was reported. Thus, according to these tests the probability of failure in the coating is higher in PLA coated HPM in comparison to the PCL coated HPM.

3.3.2.3 PCL- (AZ91 magnesium-aluminum-zinc) [53]

AZ91 magnesium, with 9 wt.% aluminum and 1 wt.% zinc, was used in both *in vitro* and *in vivo* studies by Wang et al. Improvement in the corrosion properties of magnesium implants was done through the deposition of porous polycaprolactone (PCL) coating from solutions with dichloromethane (DCM). Two different concentrations of PCL in DCM were prepared in order to fabricate coatings of varying porosity. Layer-by-layer deposition

of the polymeric coating was applied by a spraying deposition. Since the spraying device was equipped with air-flow and temperature control, the thickness, adhesion, and homogeneity of the polymeric coating was standardized. Potentiodynamic polarization test showed that the corrosion potential for both low porosity (0.8 μm-1.6 μm) and high porosity (3.2 μm- 6.4 μm) coatings increased by 1.4 V for low porosity and 1.1 V for high porosity specimens. Lower i_{corr} was also observed for the coated samples. The degradation rate of the uncoated specimens was compared with coated specimens by immersion test. Total weight loss for the uncoated metal after 2 months' immersion in SBF was approximately 17 mg. However, for the polymer coated specimens it was 3.6 mg and 6.2 mg for low porosity and high porosity coating, respectively. Inductively-coupled plasma mass spectrometry (ICPMS) illustrated 1340 ppm increment in the value of Mg ion concentrations for the uncoated specimens after 60 days of immersion in 10 ml of SBF while this value was determined 236 and 431 ppm for low porosity coating and for high porosity coating, respectively. Because the number and sizes of pores (3.6 μm by average) increased in the high porosity coating, the low porosity coating was a better corrosion barrier. In addition to the improvement of corrosion resistance, the mechanical properties of polymer coated Mg alloys have been retained. Good biocompatibility without any inflammation in *in vivo* test was an additional outcome of the study.

3.3.2.4 Polydopamine-Mg [54]

The magnesium rod substrate was coated with polydopamine (PD) with the thickness of approximately 1 μm. The magnesium rod was simply immersed in a solution of Tris (hydroxymethyl) aminomethane-buffer (pH =10) (TBS) containing dopamine. Excellent adhesion of PD to the Mg substrate was observed through ASTM "Tape Test". The Mg substrate coated with PD led to the significant improvement in corrosion resistance of Mg. The enhancement in corrosion resistance was investigated through the potentiodynamic test and using NaCl as the electrolyte. The dopamine concentrations in TBS, immersion timing, pH and dipping angle were investigated to determine the immersion parameters on the corrosion rate of Mg. The corrosion behavior of Mg coated by different immersion in TBS appears to be independent of dipping angle, pH values between 9-12 and

concentration of dopamine (addition of 2mg/ml dopamine in solution). However, immersion time had an influence on the corrosion rate of Mg, with smaller immersion times (<2 hours) leading to the most favorable results. The parameters which they led to the optimum corrosion resistance in NaCl were implemented for repeating the test in Dulbecco's modified eagle medium (DMEM). The corrosion current density decrease from ~35 µA cm^{-2} for the uncoated sample to ~14 µA cm^{-2} for the polydopamine-coated sample which was promising in DMEM as well as NaCl solution.

Table 1 illustrates an overview of relevant polymeric coating on different metal substrates. It is worth noting that most of the polymeric coatings applied for the purpose of corrosion barriers did successfully improve the corrosion resistance of the metallic substrate.

Table 3.1. Polymeric coated biomedical implants

Substrate	Polymer	Method	Thickness(µm)	Purpose	Application	Testing
SS	PEVA-PBMA	-	-	Drug eluting	stent	-
SS	SIBs	ElectroNano spray	-	Drug eluting	stent	-
Mg6Zn	PLGA	Dip coating	33 & 72	Corrosion barrier	orthopedic	*In vitro*
HPM	PLA/PCL	Dip coating	15 & 20	Corrosion barrier	Stent	*In vitro*
AZ91	PCL	Spraying	-	Corrosion barrier	orthopedic	*In vivo vitro*
Mg	PD	Dip coating	1	Corrosion barrier	Implants	*In vitro*
Nitinol	PU	Dip& brush coating	5-30	Corrosion barrier	Stent	*In vitro*
SS	parylene	CVD	2	Corrosion barrier	Implants	*In vitro*

4 Goals and hypotheses

4.1 Objectives

The objectives of this master's research include (Fig 4.1):

1. to retard the initiation of corrosion of zinc by applying a protective PLLA coating;
2. to develop a dip coating technology that produces uniform PLLA film on zinc substrate of improved zinc-PLLA adhesion;
3. to investigate the influence of the thickness of the PLLA coating on corrosion resistance and behavior of zinc substrate; and
4. to investigate the biocompatibility, cytotoxicity and bioabsorption of the PLLA-coated zinc substrate in the abdominal aorta of rats in order to explore the application of PLLA-Zn hybrid material for endovascular stent application.

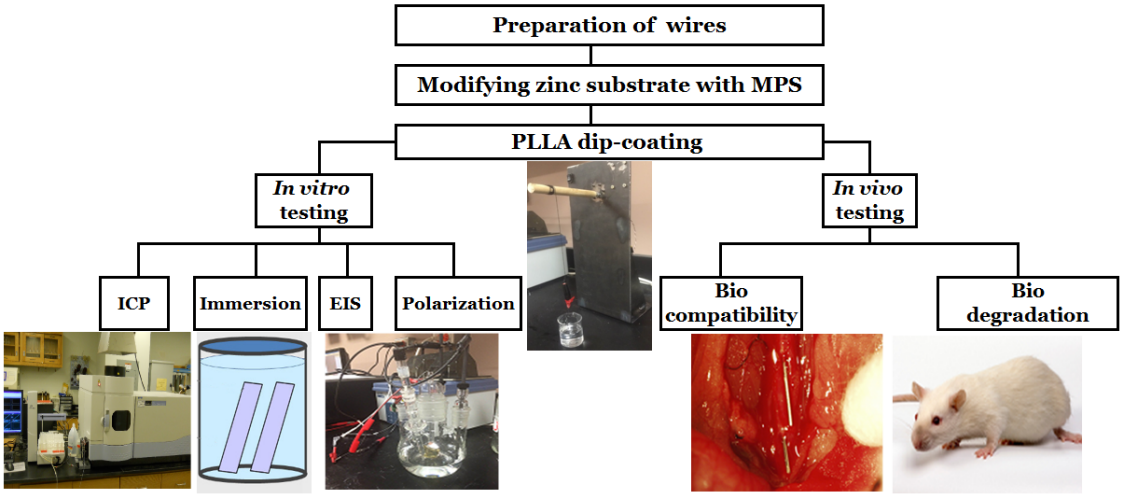

Figure 4.1. Research flow chart of experimentation under M.S. research plan.

4.2 Hypotheses

Hypothesis I: *Poly (L-Lactic-acid) (PLLA) is a suitable polymer for coating zinc substrate in terms of both corrosion behavior improvement, biodegradability, and biocompatibility.*

PLLA (Figure 4.2) is one of the FDA approved biodegradable polymers due to its history in previous successful clinical experiments, desirable degradation rate, very low or no

toxicity, high modulus and high tensile strength [30, 55, 56]. [30]. PLLA has been vastly used in tissue engineering, bone fixator, cartilage, tendon, neural, etc. [57]. However, its brittleness may restrict its usage in orthopedic and dental surgery [56].

Poly (lactic acid) (PLA) was introduced for medical application by DuPont [30]. PLA is a thermoplastic aliphatic polyester which is biodegradable and can be produced by ring opening polymerization of lactic acid. Lactic can exist in several distinct forms in PLA; (D-PLA) and (L-PLA) are the two forms which have shown promises in biomedical applications [57]. Poly (D,L-lactic acid) (PLA) is amorphous while PLLA, which is the result of the polymerization of the (L-PLA), is semi-crystalline and has great mechanical properties [58]. The methyl group which exists in PLA cause the polymer to be crystalline and as a result more hydrophobic in comparison to poly glycolic acid (PGA) which is similar to PLA [57]. Hydrophobicity is a property in the polymer which we were looking for the coating because it reduces the rate of water absorption and degradation rate as a result. It has been shown in an *in vivo* study by Suuronen et al. [59] that it takes more than five years for PLLA with high molecular weight to be absorbed completely.

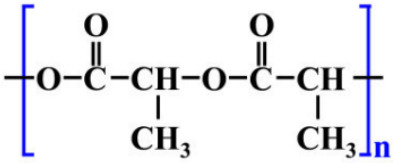

Figure 4.2. PLLA structure.

Degradation of PLLA in living organisms is through a hydrolysis reaction in which the PLLA micromolecules are broken down into degradation products, such as lactic acids, which can be metabolized and removed from the body [60, 61]. Due to the breakage of the covalent bonds between repeating units, which can occur by hydrolysis, oxidation, and enzymatic mechanism, long backbone breaks into small oligomers or monomers. Some polymerization by-products such as initiators, catalysts and stabilizers may also be released by degradation which may cause some inflammatory response in the body. The degradation starts when water penetrates the polymer. In semi-crystalline polymers like PLLA the

amorphous part of the polymer undergoes degradation before the crystalline part, thus the molecular weight of the polymer is reduced. However, the polymer still maintains its physical properties due to the bonding between crystalline regions. As water continues to penetrate to the bulk of the polymer molecular weight of the polymer reduces and finally leads to the reduction in the physical properties as well [62]

Hypothesis II: *3-(Trimethoxysilyl) propyl methacrylate (MPS) can be a suitable adhesion promoter for increasing the interfacial adhesion between zinc substrate and PLLA coating*

Because of the significant difference in the surface energy of the polymer and metallic zinc, PLLA cannot adhere easily to the zinc substrate thus the polymer and zinc want to reduce the interface area in between them in order to decrease the free energy [63]. In normal situations, bonding metals to polymers is not easy. Therefore, manipulating the interface in between them to increase the interfacial adhesion is important. Several techniques such as plasma modification, ion beam treatment, etching, anodization, surface modification [64-66] can be employed for improvement in the adhesion and durability of metal-polymer bonds.

In this study, a silane coupling agent was selected as an adhesion promoter. The ability of silane coupling agents to form a durable connection between organic and inorganic materials was the main reason for selecting this chemical to increase the adhesion. The silane coupling agent which was selected for this purpose is 3-(Trimethoxysilyl) propyl methacrylate (MPS) (figure 4.3). MPS was chosen due to its potential for binding with ZnO surface which was demonstrated by Bressy et al. [67]. Previous reports on the application of silane coupling agents in biomedical applications and their biocompatibility was another reason for the selection of MPS [68-70]. The usage of MPS in controlled drug release nanocapsules and its biocompatibility was also reported [71]. Employing two different silane coupling agents in two steps with the purpose of reducing the rapid corrosion rate of magnesium biomedical implants was also reported before [72] in which in the first step bistriethoxysilylethane (BTSE) and in the second step 3-amino-propyltrimethoxysilane (γ-APS) were applied as the anti-corrosive silane coatings for magnesium alloy implants.

Significant enhancement in the polarization resistance (from 2650 ohm cm^{-2} for the bare Mg alloy to >13600 ohm cm^{-2} for the modified Mg alloy) and decrement in i_{corr} (from 8.3 $\mu A/cm^2$ for the unmodified sample to 0.9 $\mu A/cm^2$ for the modified sample) was shown by EIS and potentiodynamic polarization tests, respectively [72]. After 6 h to 42 h of immersion of samples in SBF, the impedance was still increasing which can be interpreted as the improvement in corrosion protection of the silane coated specimens. Platelet adhesion to the two-step silane coated specimens was also investigated through conjugation of heparin to the modified Mg alloy surface by the amino groups which exist in γ-APS [72]. Reduction in platelet adhesion which can be an indication of improvement in blood compatibility was also observed with silane modification [72]. Several other observations on the influence of the silane modification on improving the corrosion resistance of other types of magnesium alloys were also reported [50, 73-75].

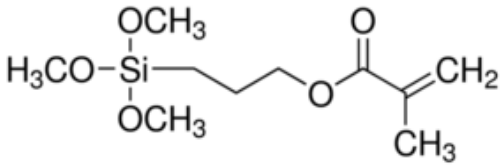

Figure 4.3. MPS structure.

The general formula for a silane coupling agent is R-$(CH_2)_n$-Si-X_3 in which R is an organofunctional group and X is hydrolysable groups such as alkoxy, acyloxy, halogen or amine. In MPS all the three X positions are occupied with three methoxy (OCH_3) groups

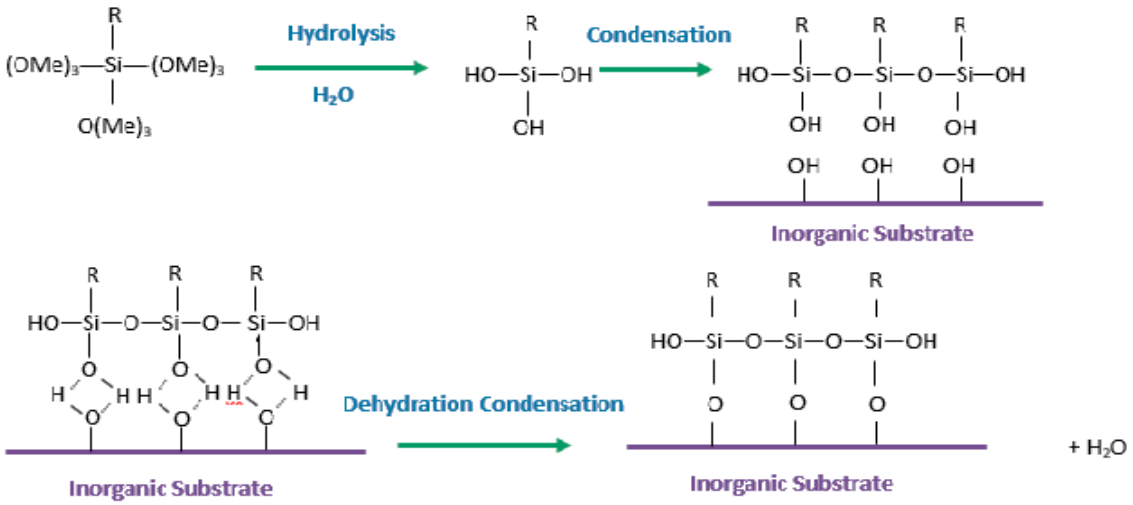

Figure 4.4. Mechanism of action of a silane coupling agent with an inorganic substrate.

and for this reason, it is called trimethoxysilane. R position is occupied with propyl methacrylate ($C_7H_{12}O_2$) group. The mechanism of reaction of the silane coupling agent
Figure 4.4. Mechanism of action of a silane coupling agent with an inorganic substrate.

with inorganic materials is shown in figure 4.4. X (alkoxy) group is illustrated as $(OMe)_3$ which in the case of MPS is equal to $(OCH_3)_3$.

For acting a silane coupling agent on the inorganic or metallic substrate first the hydrolysis of the X groups is required (figure 4.4). Water which is required for hydrolysis may be added to the silane solution, it may be existing on the surface of the substrate or it can come from the atmosphere. In the second step, oligomers are formed by partial condensation. Then the oligomers bond to the OH groups which exist on the surface of the substrate through hydrogen bonding. Finally, through a drying process, the inorganic material

adheres to the layer of the silane coupling agent by covalent linkage through a dehydration condensation reaction [76]. The X group is in charge of establishing a connection with the metallic substrate, whereas the R group is responsible for binding to the polymer via a covalent bond. The covalent bond can be formed in two ways; 1) by reaction with the finished polymer 2) by copolymerization with the monomers of the polymer which is going to bond with. In the case of MPS, propyl methacrylate ($C_7H_{12}O_2$) group reacts with PLLA.

Previous research on the adhesion of MPS to zinc oxide surface of nanoparticles along with the effectiveness of silane coupling agents in increasing the corrosion resistance and biocompatibility of bare metal specimens [50, 71-73, 75] motivated selection of MPS as an adhesion promotor between PLLA and metallic zinc substrate in this study.

Hypothesis III: *PLLA coating on the MPS modified zinc substrate can delay the early stage of corrosion*

Previous studies on PLLA and PLGA coatings on magnesium and its alloys substrate have shown an increase in the corrosion resistance of the coated samples in comparison to bare metals [36, 51, 53, 77]. However, in most of the cases, the early delamination and breakdown of the polymer coating due to its low adhesiveness to the metallic substrate caused the loss of the polymer coating corrosion protection effectiveness in the early stages of the experiment. Therefore, using an adhesion promoter such as MPS to enhance metal-polymer binding could prevent or slow down the reach of the metallic substrate by electrolytes and delay the corrosion and biodegradation.

The influence of the thickness on corrosion behavior of the metallic substrate is still unknown and under investigation. There are some reports on the influence of the thicker polymer coating in providing a better barrier to corrosion [36, 49] whereas some other reports concluded on the better corrosion resistance performance with thinner polymer coating [51] due to the increased amount of porosity and defects with thicker polymer coating and easier penetration of the electrolyte to the metallic substrate as a result. Therefore, investigating the corrosion property of the system with increasing the thickness of the coating should be considered.

Hypothesis IV: *PLLA coating on the MPS modified zinc substrate can maintain the biocompatibility of pure zinc*

Previous *in vivo* studies on implanted zinc wires within the abdominal aorta of rats demonstrated superb biocompatibility with a harmless mode of corrosion [11, 12]. After 6 months of implantation there was not any sign of significant inflammatory or toxic response. Initial hyperplasia and localized necrosis could not have been observed either.

Considering the biocompatibility and nontoxicity of PLLA and MPS (discussed under previous hypotheses) and their corrosion products, modifying zinc substrate with MPS and deposition a layer of PLLA coating cannot have a harmful effect on the biocompatibility of zinc. The *in vivo* study on PLLA coating on MPS modified zinc wire is still required to explore biocompatibility and toxicity of this Zn-MPS-PLLA system.

5 Materials and Methods

5.1 Sample preparation

5.1.1 Materials

For both *in vivo* and *in vitro* studies, zinc wires with 99.9% purity with 250 ± 25μm diameter from Goodfellow (Oakdale, Pennsylvania) were divided into 15 mm segments. Wire model studies offer several benefits in comparison with stent-based studies, such as simplicity, cost effectiveness, and ability to precisely replicate physiological environment [78]. The wires were washed ultrasonically in 200 proof ethyl alcohol for five minutes and dried prior to modification with silane coupling agent. 3-(Trimethoxysilyl) propyl methacrylate (MPS) (98% purity, 1.045g/ml) was purchased from Sigma-Aldrich as the coupling agent between the polymer coating and zinc substrate.

Poly (L-lactic-acid) (PLLA) was purchased from Natureworks LLC (Blair, Nebraska).

5.1.2 Silanization

MPS solution was prepared by mixing 95% of pure ethanol with 5% of DI water, then the pH was adjusted to 4-5 with acetic acid. MPS was added while stirring at room temperature to yield a 2% final concentration. The solution was stirred for 15 minutes at room

temperature for hydrolysis and silane formation. Zinc wires were immersed in the prepared silane solution for 30 minutes and then dried at room temperature under the hood for a day.

5.1.3 PLLA deposition

PLLA was dissolved in dichloromethane (DCM) at 1.5% wt/vol. Dip coating method was employed for polymer layer deposition among all available techniques for coating such as spray-coating, spin-coating, chemical vapor deposition, and inkjet printing that were considered in this study. Dip coating was selected since it is the simplest, easiest and most economical method for coating and material waste in this method is less than in other methods [79].

MPS-modified zinc wires were dipped into the polymer solution by a self-developed controller (figure 5.1) at room temperature. Using a self-made controller is beneficial in having an exact extraction velocity to have a uniform coating along the substrate. Because withdrawal velocity is constant a uniform and consistent coating of desirable polymer thickness was achievable.

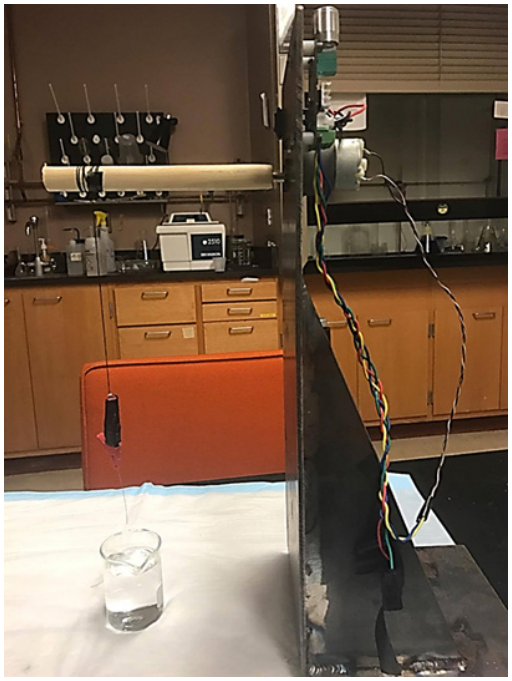

Figure 5.1. Self-made controller for polymer deposition.

In this study, 10 mm/s was the adjusted speed for withdrawing the wires. The coated specimens were dried in an oven at 35°c for a day and the polymer coating forms on zinc substrate after evaporation of the solvent. Figure 5.2 illustrates the procedure for polymer coating deposition. Specimens were cleaned with pure ethyl alcohol after PLLA deposition.

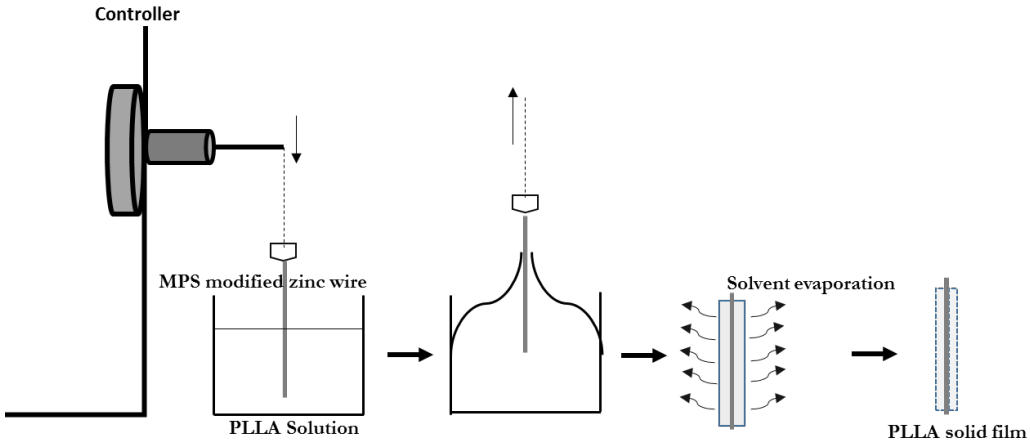

Figure 5.2. PLLA deposition procedure.

The concentration of the dissolved PLLA in the solvent and withdrawal velocity are the two parameters which can be altered to get different thickness of polymer on the substrate [80]. Thus, to deposit various coatings of PLLA on modified zinc substrate 1.5, 5 and 15 grams of PLLA, was dissolved in 100 ml of DCM solvent. Two different velocities for extracting the wires from the solutions were also assigned (10 mm/s and 20 mm/s). Therefore, three sets of samples were prepared; 1.5 w/v% PLLA with 10 and 20mm/s withdrawal velocity, 5 w/v% PLLA with 10 and 20 mm/s withdrawal velocity. 15 w/v% PLLA with 10 and 20 mm/s withdrawal velocity.

5.2 Surface characterization

5.2.1 Contact angle measurements

To investigate the presence of the silane coupling agent on the zinc substrate contact angle goniometry was performed. The contact angle is defined as the angle which is formed

between the liquid-solid interface and the tangential line to the liquid droplet on the solid surface. For our experiment water was used as the liquid. The measured angle can be an indicative of the wettability of the surface. Angles less than 90 degrees indicates a surface with high wettability whereas contact angles greater than 90 degrees can be indicative of low wettability of the surface [81].

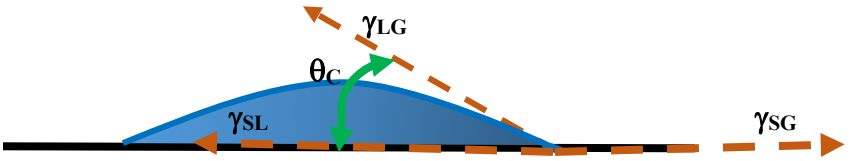

Figure 5.3. Schematic of a liquid drop and the contact angle of a liquid with a solid.

The shape of the droplet on a solid surface is dictated by competition between capillary and gravity forces (Figure 5.3). A balance between interfacial tensions in three-phase system and resulting contact angle (θ) is summarized by Young's equation (1):

$$\gamma_{LG}\cos\theta_c = \gamma_{SG} - \gamma_{SL} \qquad (1)$$

Where γ_{LG} , γ_{SL}, and γ_{SG} are surface tension of liquid, solid-liquid interfacial tension and solid surface tension, respectively.

Since measuring the contact angle on the surface of the wires is impossible, zinc sheets were used for this purpose. In order to have a smooth zinc's surface, 1cm x 1cm zinc sheet was first mounted in a two-part epoxy and then the exposed surface of zinc was grounded and polished with 600 grit SiC paper and 6 and 1 μm diamond. The procedure for silanization was performed according to subsection 5.1.2.

5.2.2 Electron imaging

The polymer coating was characterized pre and post corrosion by the use of Field Emission Scanning Electron Microscope (FESEM) and SEM. The thickness of the deposited PLLA coatings was also measured by electron imaging with the following procedure.

After preparing the samples (1.5 w/v% PLLA with 10 and 20mm/s withdrawal velocity, 5 w/v% PLLA with 10 and 20 mm/s withdrawal velocity. 15 w/v% PLLA with 10 and 20 mm/s withdrawal velocity), they were mounted on a SEM sample holder and they were carbon coated afterwards to prevent charging of specimens and improve secondary electron emission and conductivity. JEOL JSM-6400 conventional SEM at 5 kV accelerating voltage was used to image an MPS modified zinc and PLLA coated MPS modified Zn wires with 450× magnification. After obtaining the images, Image J software was used to measure the diagonal length of the MPS modified Zn wire and the diagonal length of the MPS modified PLLA coated wire. A five-time average of width was taken using the scale given on SEM image by Image J software and then the average was divided into two for measuring the thickness of the coating

Following equation was used to calculate the thickness (h);

$$h = \frac{D-d}{2} \tag{2}$$

In which D is the diagonal length measured after polymer deposition and d is the diagonal length measured before polymer deposition. Figure 5.4 illustrates the procedure for measuring the thickness of PLLA coating.

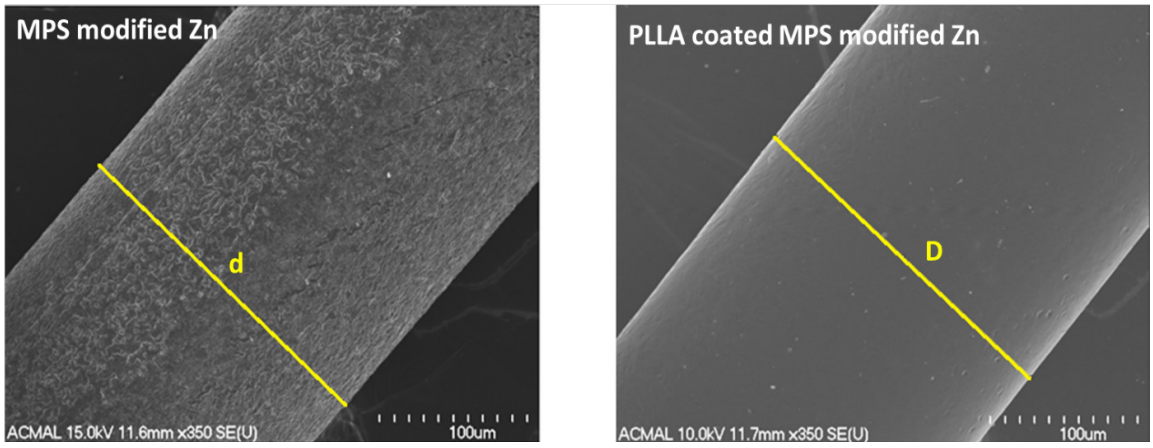

Figure 5.4. PLLA coating thickness measurement method.

To obtain images with higher magnification for a better evaluation of the coating a Hitachi S-4700 FESEM, operated at 5 kV of accelerating voltage was used.

To verify the uniformity of the polymer coating after deposition and in order to investigate the stability and durability of PLLA after different immersion times in simulated body fluid (SBF) solution and after 14 days of being in the abdominal aorta of rats, FESEM and SEM techniques were used. FESEM was used for the specimens with thick polymer coating while SEM was used for the samples with a thin polymer coating. These techniques were also employed for measuring the thickness of the polymer coating.

Environmental scanning electron microscope (ESEM) was used to investigate the presence of the corrosion products on the 3, 4.5, and 6 months *in vivo* corroded wires. Therefore, after imaging the cross sections of the wires with SEM, Philips XL40 ESEM was used to examine the corrosion products on different samples and compare them.

5.3 Corrosion rates determination

Investigation of the effectiveness of PLLA coating on the corrosion rate of zinc was performed both outside and inside a living organism (*in vitro* and *in vivo*). To measure the corrosion rate several methods such as weight loss, thickness measurements, chemical analysis of solution (only applicable for the *in vitro* test), electrochemical techniques and etc. can be carried out [82]. For the purpose of our study, change in the cross section or radius of the specimens' after different immersion times in SBF solution for *in vitro* test and after various exposure times to abdominal aorta of rats for *in vivo* test was measured. The procedure for measuring the reduction in the cross section of the wires will be explained in subsection 5.3.1.1.1. Different electrochemical techniques (potentiodynamic polarization and EIS tests) were also carried out to estimate the corrosion rate of the polymer coated samples and compare the results with the other *in vitro* tests and *in vivo* test.

5.3.1 In vitro Studies

5.3.1.1 Immersion Test

Immersion test is one of the techniques for assessing the corrosion behavior of the candidate material [82]. In a simple immersion test, small sections of the under examination material are immersed in the test medium that can simulate the corrosion damage. After exposure of the sections to the test medium for a certain amount of time, the loss of weight or reduction in the cross section of the material can be measured. The pH variation of the test medium or change in the concentration of different elements in the solution can also be conducted to evaluate the corrosion properties of the candidate material.

A simulated body fluid (SBF) with elements, ion concentrations and the pH close to human body plasma was selected for our experiment. NaCl, $NaHCO_3$, KCl, Na_2HPO_4, $MgCl_2.6H_2O$, $CaCl_2.2H_2O$, Na_2SO_4 are the constitution of the prepared SBF. Table 5.1 compares the SBF and human blood ion concentrations. After preparing the solution in order to inhibit bacterial colonization, 1% volume of a solution containing penicillin at 10,000 units mL^{-1} and streptomycin at 10 g/L (Sigma Aldrich, St. Louis, MO) was added to the solution. The pH of the media was 7.57 ± 0.02.

Table 5.1. Ion concentrations in the human body plasma and simulated body fluid.

Ion	Blood plasma/mM	Revised SBF/mM
Na^+	142	160
K^+	5	4
Mg^{2+}	1.5	1
Ca^{2+}	2.5	2.5
Cl^-	103	142
HCO^{3-}	27	26
HPO_4^{2-}	1	1
SO_4^{2-}	0.5	0.5
pH	7.2-7.4	7.4

Two different thicknesses of the PLLA coating was deposited on the modified zinc wires (1 and 3 μm) with the procedure which was described in subsection 5.3.1. Four 15 mm uncoated zinc wires, 4 MPS modified 1 μm PLLA coated zinc wires and 4 MPS modified 3 μm PLLA were cleaned with ethanol and irradiated with ultraviolet light to sterilize the surface and they were individually submerged into 40 ml disposable test tubes containing SBF and incubated at 37°C and 5% CO_2 from 1-14 days. The media was not replaced during the time period. One 15 mm wire was removed from each set of samples after 5, 7, 11 and 14 days to monitor the change in cross-sectional area (CSA) reduction. Penetration rate for each sample was also calculated by using the change in CSA following established protocols [9, 38].

5.3.1.1.1 Cross-sectional analysis

To analyze the change in cross sections of the wires after being immersed in SBF for different time intervals, multiple cross sections of the wires were prepared by the following procedure [11];

I. Placing the wire in a plastic sample clip
II. Placing the clip which is holding the wire into a silicon tube (inner diameter of the tube is approximately 8 mm) and adjusting it in a vertical position
III. Adding two-part epoxy resin into the tube and waiting for 12 hours for the epoxy to be cured
IV. Removing the cured epoxy which has the clip and the wire from the tube
V. Cutting the epoxy transversely and obtaining 8-10 cross sections (Each section was almost 0.5-1 mm thick)
VI. Sticking the cross sections on a polystyrene sheet
VII. Sticking the polystyrene sheet on the bottom part of an epoxy mounting cup
VIII. Pouring two-part epoxy into the cup and waiting 12 hours for the epoxy to be cured
IX. Taking out the cured epoxy from the cup and removing the polystyrene sheet
X. Grounding the newly exposed surface with 600 grit SiC paper and then polishing it with 6, 1 and 0.5 μm diamond

XI. Carbon coating the embedded sections to creating a conductive layer of metal on the sample to improve imaging

XII. Imaging the section with a JEOL JSM-6400 conventional SEM at 20 kV accelerating voltage and using its back-scattered electron (BSE) detector. 250× was the nominal magnification to image the cross sections of each wire

XIII. Performing CSA analysis with the Image J software package

The employed process for calculating the CSA reduction by Image J software is illustrated in figure 5.5. By thresholding the bright part of the wire which is zinc was selected to select the brightest pixels and then measured. The total area of the wire was also approximated and measured. By subtracting the two measured area and dividing it by the total area the CSA reduction was calculated.

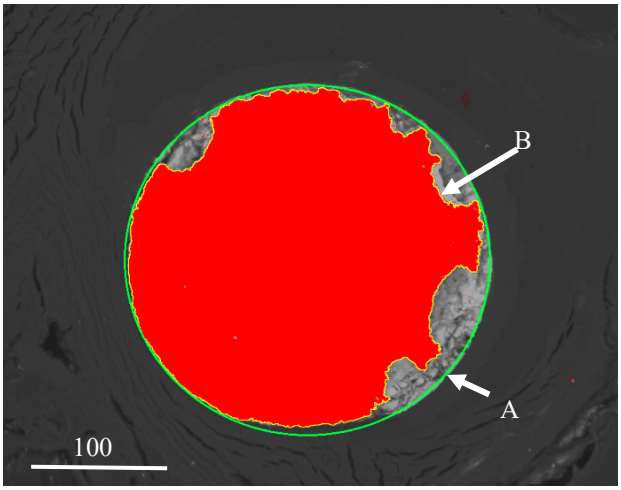

Figure 5.5. BSE image of the cross section of a wire embedded in resin; The original cross section of the wire is marked with a green ellipse (A) and the remained zinc wire is after being corroded is marked with yellow (B).

5.3.2 Electrochemical tests

Electrochemical experimental methods can be used to evaluate the corrosion behavior of metals since corrosion is an electrochemical process at the interface between metal and an electrolyte solution in which electrons are released by the corroding metal (oxidation) to the solution (electrolyte) and gained by some elements (reduction) in the solution such as

hydrogen or hydroxide ions. The flow of electrons from the metal to the solution creates an electric current which can be measured and controlled electronically. The unique corrosion characteristics for each metal/solution system enables us to use this technique to evaluate the corrosion behavior. Potentiodynamic polarization and electrochemical impedance spectroscopy (EIS) are the two techniques which were used for the purpose of our research to acquire useful information such as corrosion rate and corrosion mechanism of the PLLA coated modified zinc wires. The corrosion rates which are calculated by this method should be compared with the corrosion rates which were calculated by other methods.

5.3.2.1 Potentiodynamic polarization test

The potentiodynamic polarization test is performed by changing the potential of the working electrode (Specimen) and monitoring the current constantly. The working, reference, and counter electrodes are connected to a potentiostat which can vary the DC potential of the metal of interest and measure the current. The three-electrode polarization cell setup is shown in figure 5.6; where the PLLA coated modified zinc wire is the working electrode, saturated calomel electrode (SCE) is the reference electrode and graphite is the counter electrode. Polarization was carried out in a 600 ml SBF at 37.5 ºC while stirring the solution.

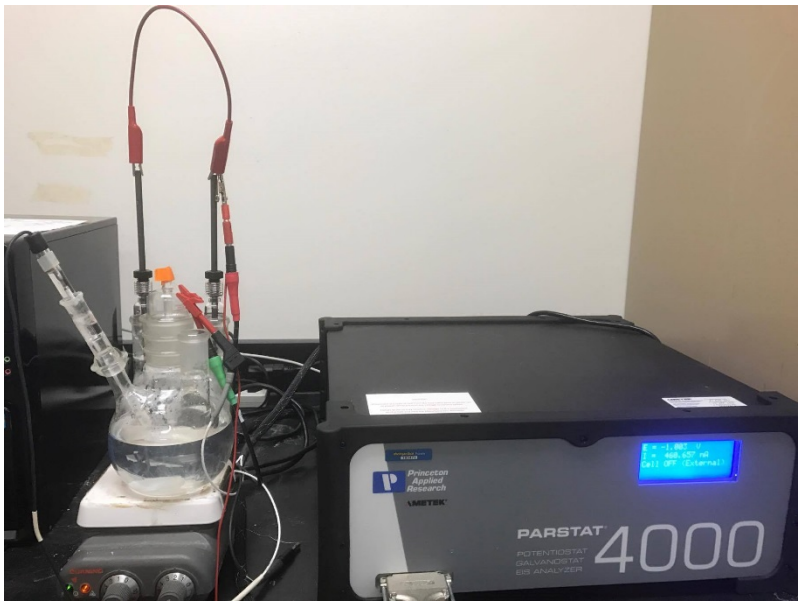

Figure 5.6. Three electrode cell set up for potentiodynamic polarization test.

The length of the exposed wire to the solution was 30 mm approximately. By having the diameter of the wires, the exposed surface area of the wires to the electrolyte was calculated by the following equation.

$$A = 2 \pi r h + 2 \pi r^2 \quad (3)$$

The diameter of the wire is so small that the $2 \pi r^2$ is negligible. Therefore, the exposed surface area can be calculated as; $A = 2 \pi r h = 2 \pi (0.125) (30) = 23.5 \text{ mm}^2 = 0.235 \text{ cm}^2$.

The electrochemical measurements were performed by the PARSAT 4000 potentiostat/galvanostat joined with the Versa Studio software package. The polarization curves were measured at a scan rate of 1 mVs^{-1} in a SBF solution with the pH of 7.54 at 37ºC.

After obtaining a steady-state, the applied potential versus log I i I were plotted to present the potentiodynamic polarization data to calculate the corrosion current which is essential in calculating the penetration rate. The approximated values of corrosion potential and

corrosion current densities were determined from the Tafel slopes by intersecting the anodic and cathodic Tafel slopes.

The comparison between corrosion potentials of the uncoated wire with the modified PLLA coated wires can be indicative of potential of the wires to be corroded. More negative corrosion potential means higher tendency of the substrate to be corroded and lose electrons. Obtained values for corrosion current was used to calculate the corrosion rate (CR) in terms of penetration rate by equation 4;

$$\mathrm{CR} = \frac{i\ corr\ (K)\ (EW)}{\rho} \tag{4}$$

where: CR was calculated in mm/yr by substituting i_{corr} in $\mu A/cm^2$, density (ρ) in g/cm^3 and k, which is a constant that defines the units for the corrosion rate, as 3.27×10^{-3} mm g/ µA cm yr. EW is the equivalent mass of the corroding species.

5.3.2.2 Electrochemical impedance spectroscopy

EIS test is performed by applying an AC potential (sinusoidal potential excitation) to the electrochemical cell and measuring the current in the cell. The response to the applied sinusoidal potential is an AC current signal with phase shift of φ [82]. E_t which is the excitation signal is expressed as;

$$E_t = E_0 \sin(\omega t) \tag{5}$$

In which ω is the radial frequency. The relationship between ω (radians/second) and frequency (Hz) is;

$$\omega = 2\ \pi\ f \tag{6}$$

The AC response current signal is equal to;

$$I_t = I_0 \sin(\omega t + \varphi) \tag{7}$$

According to Ohm's law, in DC current the resistance (R) can be calculated by dividing E by I. Impedance which is the ac equivalent of resistance can be calculated by equation 8 [83];

$$z = \frac{E}{I} = \frac{E_0 \sin(\omega t)}{I_0 \sin(\omega t + \varphi)} = Z_0 \frac{\sin(\omega t)}{\sin(\omega t + \varphi)}$$

(8)

Parameters such as slow electrode kinetics, slow chemical reactions and diffusion can impede the flow of electrons from anode to the cathode. These impeding factors can be analogous to the resistors, capacitors and inductors in a real ac circuit [84].

From Eulers relationship, it is known that,

$$\exp(j\varphi) = \cos\varphi + j\sin\varphi \tag{9}$$

Therefore, potential, current and impedance can be expressed as complex functions according to equation 10, 11and 12 respectively [83].

$$E_t = E_0 \exp(j\omega t) \tag{10}$$

$$I_t = I_0 \exp(j\omega t - \varphi) \tag{11}$$

$$Z(\omega) = \frac{E}{I} = Z_0 \exp(j\varphi) = Z_0(\cos\varphi + j\sin\varphi) \tag{12}$$

5.3.2.2.1 Data presentation in EIS [83-85]

According to equation (11) the z (ω) is composed of a real and an imaginary part. One way for presenting the EIS data is to plot the real part of the impedance on X-axis against the imaginary part of the impedance on Y-axis and we get a "Nyquist plot ". Figure 5.7 represents the Nyquist plot for a simple circuit equivalent circuit (Randles cell).

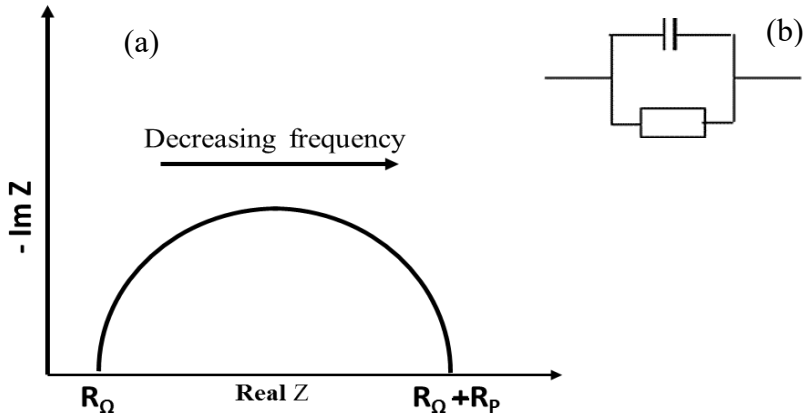

Figure 5.7. a) Nyquist plot and b) its simple equivalent Resistor Capacitance (RC) circuit.

In a randles cell the high frequency limit (rightmost end of the circle) approximates the ohmic resistance of the solution, whereas the leftmost end of the circle (low frequencies) approximates a pure resistance (polarization resistance plus ohmic resistance) [84]. Therefore, polarization resistance (R_p) can be calculated by subtracting the value of the leftmost end of the circle from the rightmost end of the circle. Polarization resistance happens when the potential on the electrode is different form its equilibrium potential [84]. Polarization resistance in an electrochemical cell acts like a resistor in a real electrical circuit. This is referred to polarizing the electrode which causes the current to flow by the electrochemical reactions that happens on the electrode surface. Kinetics of the reactions and the rate of their diffusion can affect the amount of the current. The higher the value of polarization resistance the slower the corrosion rate is.

The Bode plot is another way of presenting the EIS data in which it calculates the absolute value of the impedance and the phase shift (φ) as a function of frequency. The dependence of impedance on the frequency can be understood with Bode plot which is one of the advantages of Bode plot over Nyquist plot [83, 84]. Figure 5.8 represents a typical Bode plot for a simple electrochemical system.

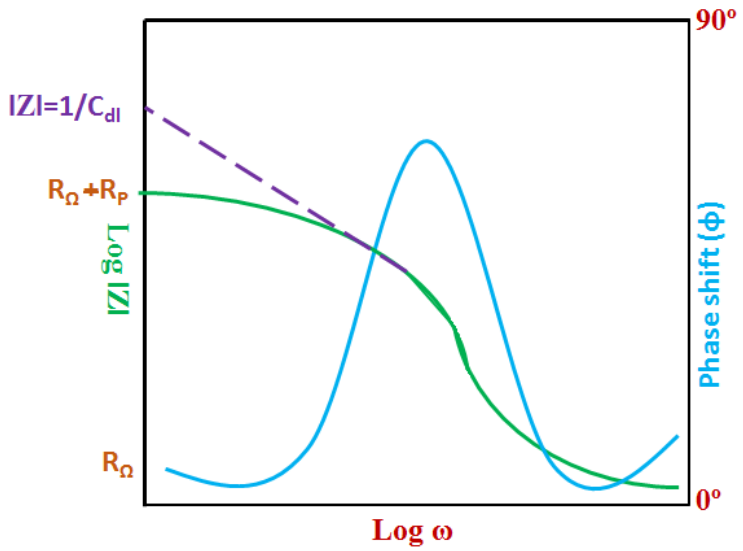

Figure 5.8. Bode plot for a simple electrochemical cell.

The values for R_Ω and $R_\Omega + R_P$ can also be read by Bode plot (figure 5.8). At intermediate frequencies extrapolating the line to the log|Z| axis at logω=0 (ω=1) gives the value for absolute impedance[84].

By taking the inverse of the absolute value of the impedance double layer the capacitance (C_{dl}) can be calculated. Double layer capacitance occurs at the interface between the working electrode and its surrounding electrolyte. When the ions in the electrolyte are adsorbed by the electrode surface, an insulating space is formed which separates the working electrode from the charged ions. Hence, in this situation the working electrode immersed in an electrolyte can behave as a capacitor in the real electrical circuit [83].

The initial polarization resistance of the coated and uncoated samples was measured after 1 h immersion in SBF to ensure a stable potential of the sample. By comparing the initial polarization resistance, impedance and the shape of the Nyquist plot for the coated specimens we can achieve to an initial evaluation of the influence of the modification and coating. Also, in order to monitor the change in the MPS modified PLLA coated specimens they were immersed in SBF for different time intervals (3,5, and 10 days) at 37ºC. After different immersion times in SBF, EIS analysis was performed on the specimens to investigate the change in polarization resistance and impedance of the specimens. SBF with the pH of 7.54 at 37ºC was used as the electrolyte. The shape of the Nyquist plot can also be an indicative of the stability or deterioration in the coating. Nyquist plots for different categories of performance of a deposited coating and their equivalent circuits are illustrated in figure 5.9. [83]

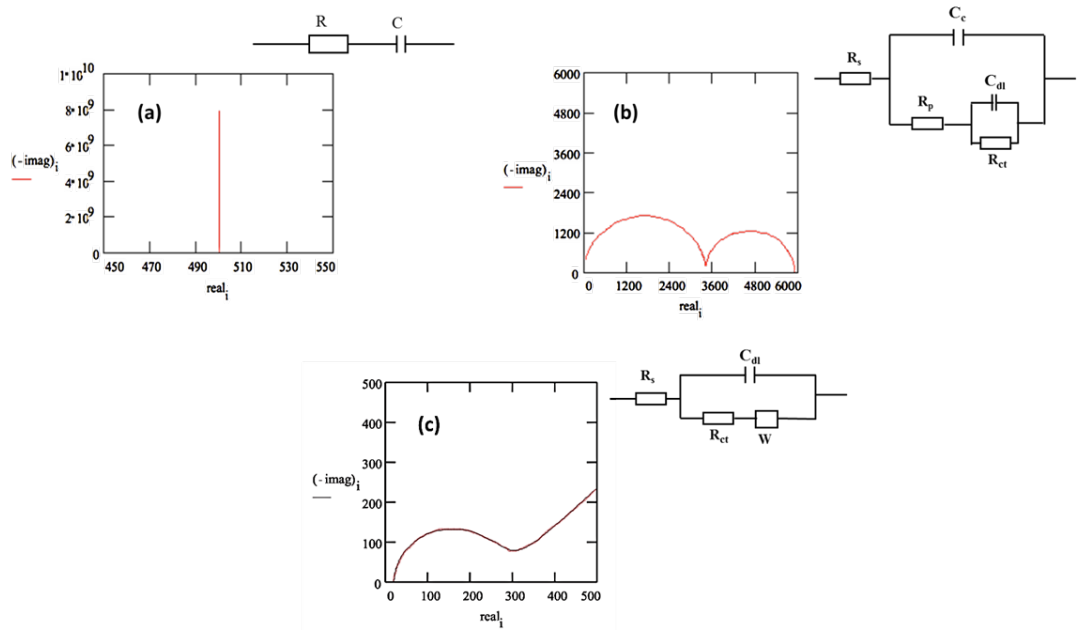

Figure 5.9. Different types of Nyquist plots and their possible simulated electric circuit for a) an excellent b) a failed c) mixed kinetic and charge transfer control coating.

R_{ct} in figure 5.9b and c, is the charge transfer resistance. Certain resistance is associated with the process of transferring the electrons, which are produced at the metal surface, to the cathodic site of the reaction (transferring electrons to the hydrogen ions to produce hydrogen gas for instance). This resistance that impede the flow of electrons to the cathodic site in called charge transfer resistance [84]. R_{ct} is an indicative of the corrosion process and the electrochemical behavior at the metal surface. The higher the value for R_{ct} the lower the corrosion rate is [84].

W in figure 5.9c is the Warburg impedance. Diffusion of a reactance such as hydrogen ion towards the working electrode or the diffusion of the products, which are produced on the working electrode substrate, away from the electrode surface affect the rate of the electrochemical reaction. This effect is magnified when the working electrode is covered with reaction products, adsorbed solution components or a coating. When the electrochemical reaction is mostly controlled by the diffusion rate of species the impedance

is called Warburg Impedance. If the electrochemical reaction is a diffusion-controlled reaction, then the current is 45 degrees out of phase from the applied potential. In case of a resistor the phase shift between the current and the potential is zero, whereas for a capacitor the phase shift is 90 degrees. Therefore, the behavior of Warburg impedance is in between a resistor and a capacitor and no simplified electrical equivalent exists for it [84].

5.3.3 Inductively coupled plasma optical emission spectroscopy

ICP test was carried out with a Perkin Elmer optima 7000DV ICP-OES instrument after immersing the uncoated and MPS modified PLLA coated Zn in 15 ml of SBF at 37.5 ºC at different time points to monitor the release of Zn ions of the polymer coated and uncoated samples. At six different time points (i.e. 1, 3, 7, 11 and 14 days) the release of Zn ion was measured.

5.3.4 In vivo studies

To prove the suitability of the polymer coated MPS modified Zn to be used as a bioabsorbable material, the biocorrosion, bioabsorption, biocompatibility and cytotoxicity of the specimens were investigated using Sprague Dawley rats. All animal tests have been approved by the animal care and use committee of Michigan Technological University.

15 mm Zn wires with the diameter of 0.25 mm were MPS modified and then coated with PLLA with the thickness of 1 μm. These samples were implanted into the abdominal aorta of rats following previously established protocols [9]. We chose to use a paired sampling method with two samples implanted in each rat. One wire was used for corrosion analysis and the other one for histological analysis.

After 0.5, 3, 4.5 and 6 months, the rats were euthanized by the use of carbon dioxide asphyxiation and the wires were removed from the rat aortas for corrosion and histological analysis. Before performing the corrosion analysis, the wires were preserved in 200 proof ethanol for five days to preserve the corrosion layer. Corrosion analysis was carried out by calculating the cross-sectional area reduction and the penetration rate of the explanted wires by the procedure which was explained in subsection 5.3.1.1.1. Investigating the

surface morphology of the wires after explanting the wires could be carried out by FESEM only on the wire which remained in the abdominal aorta for two weeks. The adherence of the tissue to the wires which were explanted after two weeks prevented surface characterization.

The histological analysis was also performed on the wires which remained implanted in the aortas and were snap frozen in liquid nitrogen [9]. The samples were stored at -80 ºC until they could be stained with hematoxylin and eosin (H&E) and mounted in the Permount solution to be imaged by a bright field microscope (Olympus BX51, DP70) [9].

In another *in vivo* experiment, the MPS modified Zn wires were coated with 3 µm and 12 µm PLLA coating to investigate the influence of the thickness of the coating on the degradation rate of the wires in a living organism. The 3 and 12 µm PLLA coated specimens were implanted in the abdominal aorta of rats for two weeks. After two weeks the wires were explanted. The corrosion and histological analysis were performed on them as it was described by Pierson *et al* [9]. Surface characterization was also performed for these wires by FESEM.

6 Result and discussion

6.1 Surface characterization

Contact angle measurements were carried out to determine the formation of the silane layer on the zinc substrate and the formation of the PLLA coating on the modified zinc sheet. The images of water droplets on samples are presented in figure 6.1.

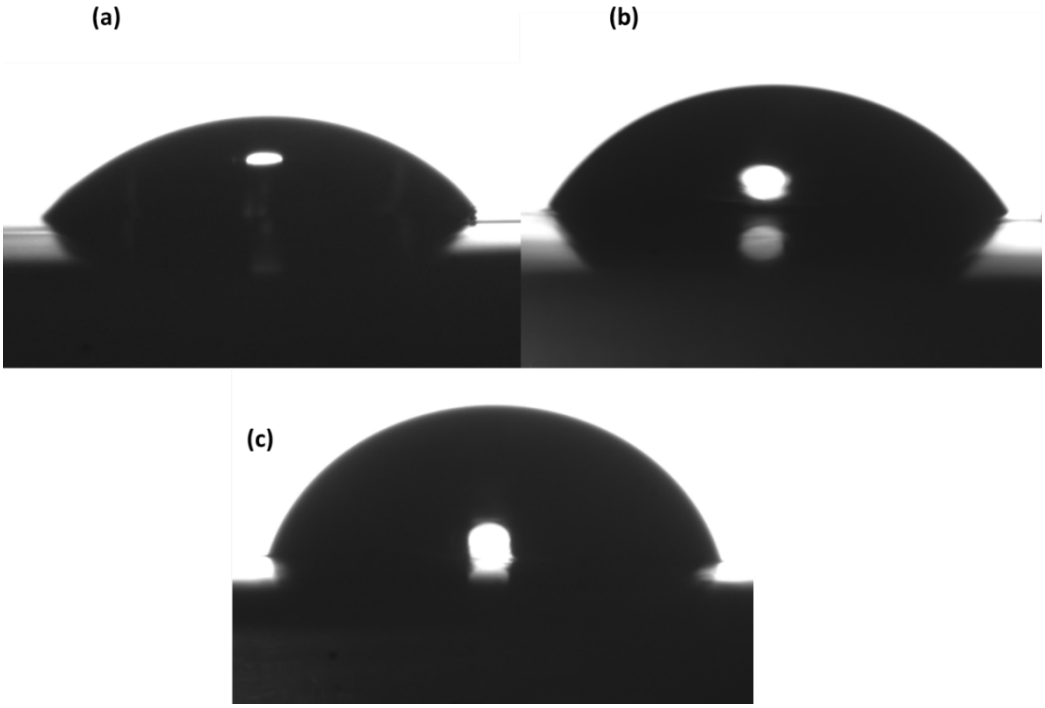

Figure 6.1. Images of water droplets on a) bare Zn b) MPS modified Zn and c)1 µm PLLA coated MPS modified Zn.

Figure 6.2 illustrates the measured contact angles for each specimen which have been replicated six times. The lowest contact angle (52 ± 2º) belongs to the pure zinc substrate whereas the MPS modified Zn substrate has the highest contact angle (73 ± 2º) suggesting that Zn is the most hydrophilic substrate between the three specimens. Therefore, by applying MPS and PLLA coating we made the Zn substrate less hydrophilic which can be beneficial in obstructing the water uptake by the substrate and reduction in the degradation rate as the consequence.

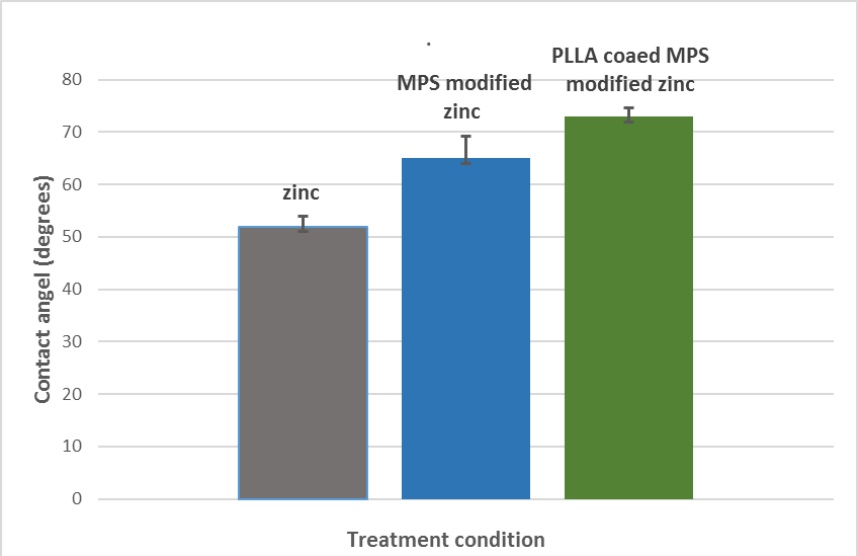

Figure 6.2. Contact angle measurements for different surface treatments.

FESEM and SEM were used to measure the thickness of the deposited coating and to characterize the morphology of the zinc wire surface after PLLA deposition as well as after *in vitro* and *in vivo* corrosion studies to evaluate the uniformity and stability of the polymer coating. The change in the PLLA coating thickness on the Zn wires and the change in the surface morphology of the wires were investigated by altering the concentration of the PLLA in the DCM and withdrawal velocity.

Figure 6.3 illustrates the SEM images of PLLA coated modified Zn wires. SEM images revealed a uniform, smooth and homogeneous PLLA coating on all the Zn wires. However, for the thicker polymer coating (15 w/v% PLLA in DCM) a porosity was observed. The wires were also imaged under FESEM to characterize the surface features at high magnification (figure 6.4). As shown in figure 6.4c, the thicker coating had a porous

structure. Image analysis revealed that the porous channels covered about 37 ± 5% of the surface and diameter of the opening was 0.3 ± 0.01 μm.

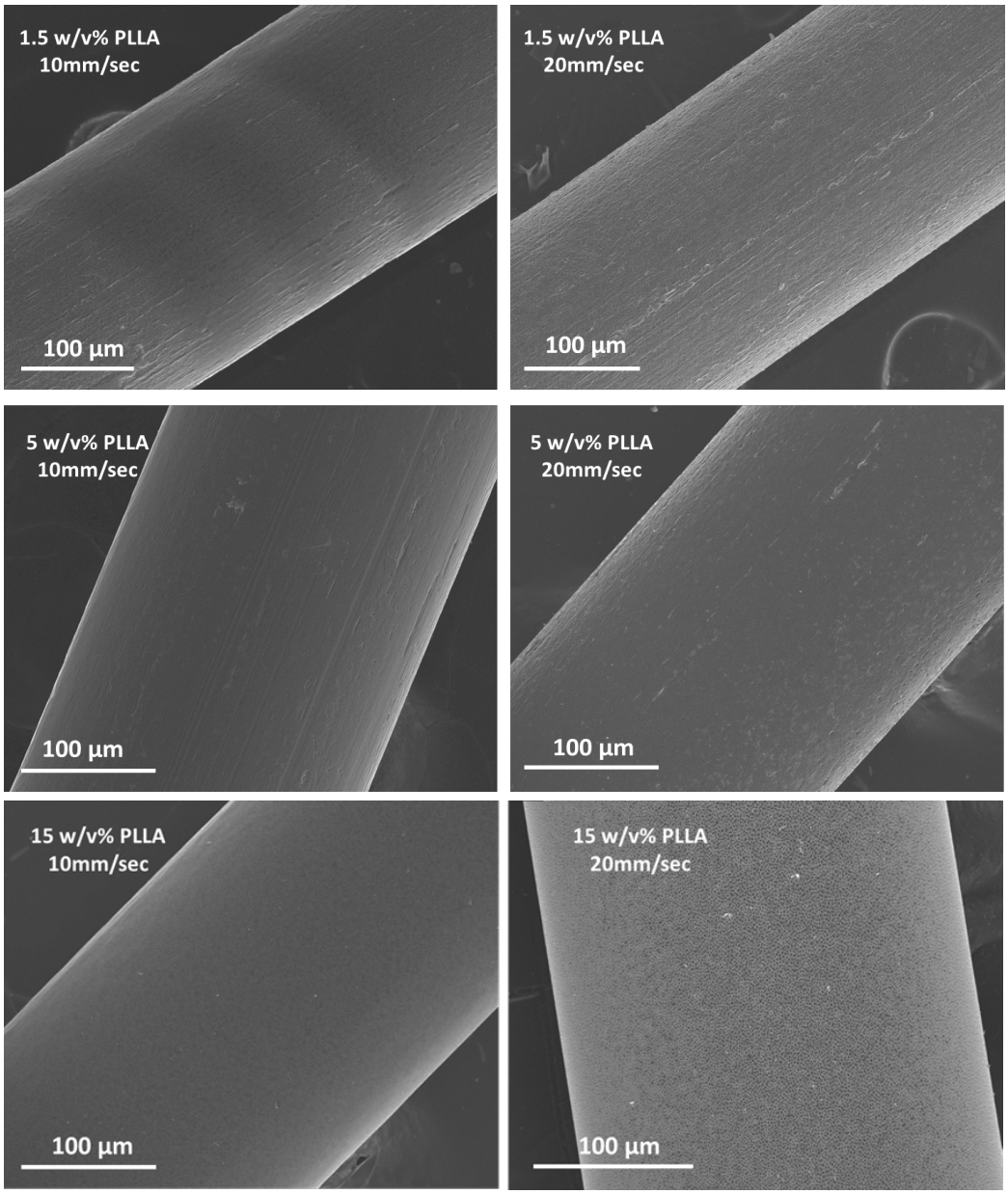

Figure 6.3. SEM images of the surface of the PLLA coated modified Zn wires. The coatings were made from two different PLLA concentrations in DCM and two different withdrawal velocities, therefore, having different thicknesses.

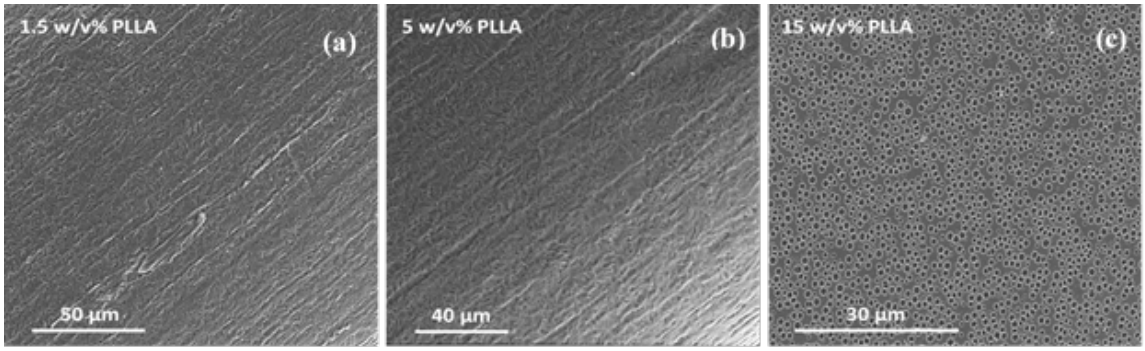

Figure 6.4. FESEM images of the surface of the PLLA coated modified Zn wires. The withdrawal velocity was 20 mm/sec for all the wires.

The presence of porosities on the surface of the wire in figure 6.4(c) can be detrimental for the metallic substrate in terms of increasing the rate of electrolyte penetration throughout the openings and making the metallic surface readily accessible to the electrolyte. It can lead to a faster degradation of the polymer and the metallic substrate as the consequence. Faster deterioration of the polymer coating in a thick polymer coating compare to a thin coating which was observed before by Li *et al.* [51] and was referred as due to the presence of flaws and voids in the thicker polymer coating.

The thickness of each of the deposited PLLA coating was measured by the method which was described in the subsection 5.2.3. The estimated thicknesses are presented in table 6.1.

Table 6.1. Estimated PLLA thickness on the modified Zn wires with various PLLA concentration in DCM and various withdrawal velocities.

PLLA Concentration in DCM (w/v%)	Extraction velocity (mm/sec)	Coating Thickness(μm) ± Standard error
1.5	10	0.9 ± 0.2
	20	2.6 ± 0.3
5	10	3.2 ± 0.1
	20	5.7 ± 0.6
15	10	4.3 ± 0.6
	20	12.1 ± 0.4

Our results show that the increase in the polymer deposition velocity (directly correlated with a velocity of removal of the wires from the solution) and an increase in the concentration of PLLA in DCM lead to the increase of PLLA thickness on the wires. With higher withdrawal velocity more liquid pull out of the solution and this results in a thicker polymer coating [80].

6.2 *In vitro* tests results

6.2.1 Immersion test

Uncoated Zn, Zn-MPS-1μm PLLA coated and Zn-MPS-3μm PLLA coated specimens were immersed in SBF in an incubator at 37.5ºC and 5% CO_2 for 1-14 days. After 5,7,11 and 14 days, one sample from each set was removed to monitor and compare their CSA reduction and PR. By analyzing the BSE images of the cross sections of the samples (6-7 cross sections per wire) (figure 6.5) the values for CSA reduction and PR could be calculated. The calculated values are reported in table 6.2.

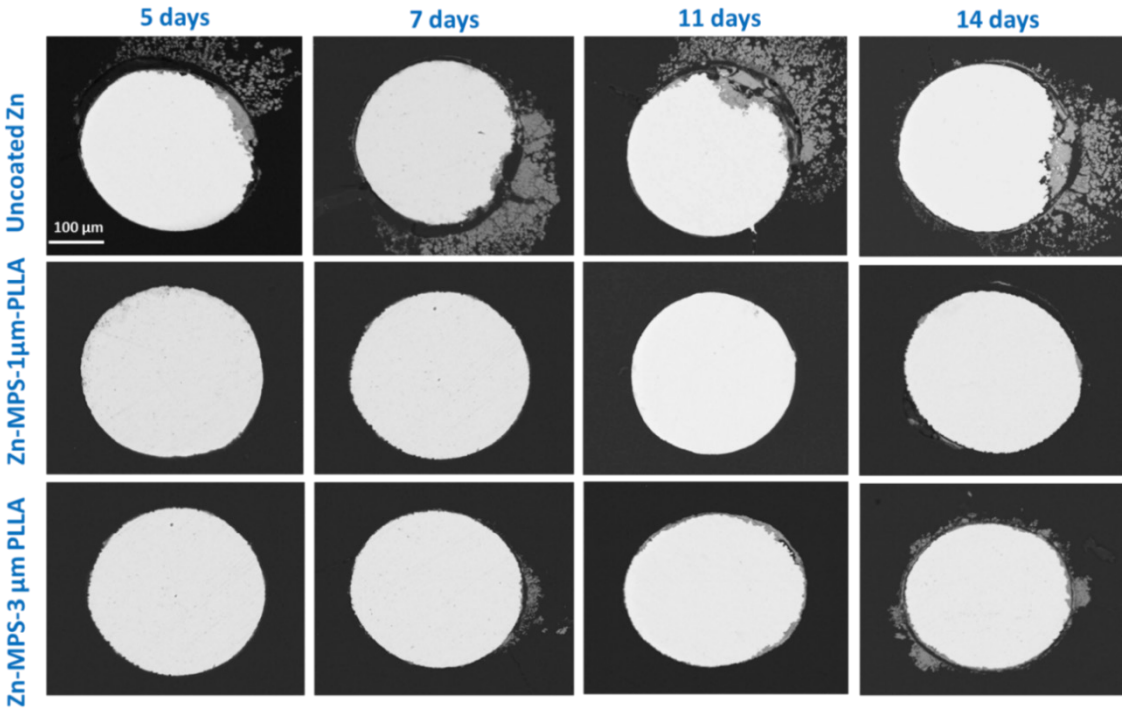

Figure 6.5. Representative BSE images from uncoated and PLLA coated wires with two different thicknesses after different exposure times to SBF.

Table 6.2. Calculated PR and CSA reduction for uncoated and coated specimens after different immersion times in SBF.

Substrate	Immersion time (days)	PR ± Standard error (µm/year)	CSA Reduction ± Standard error (%)
Pure zinc	**5**	**280 ± 146**	**6 ± 3**
	7	**355 ± 162**	**10 ± 4**
	11	**256 ± 68**	**12 ± 3**
	14	**201 ± 63**	**12 ± 4**
Zn-MPS-1 µm-PLLA	**5**	**29 ± 10**	**1 ± 0**
	7	**19 ± 4**	**1 ± 0**
	11	**44 ± 6**	**2 ± 0**
	14	**38 ± 6**	**2 ± 0**
Zn-MPS-3 µm-PLLA	**5**	**25 ± 8**	**1 ± 0**
	7	**43 ± 10**	**1 ± 0**
	11	**16 ± 5**	**1 ± 0**
	14	**38 ± 13**	**2 ± 1**

The CSA reduction and PR of specimens as functions of immersion time are presented in figures 6.6. In accordance to these figures, CSA reduction and PR of the pure zinc wire is more than all the polymer coated MPS modified Zn wires. After 7 days of incubation, the uncoated Zn specimen had the highest penetration rate and CSA% reduction in comparison to the polymer coated specimens. The penetration rate for pure zinc wire continued to increase noticeably after 7 days of the experiment whereas it increased slightly for thicker polymer coating and decreased for the thinner polymer coating. At day 14, the uncoated Zn wire had the highest PR and CSA% reduction, whereas the penetration rate for the MPS modified 1 and 3 µm PLLA coated Zn wires were noticeably less (~ 160 µm/year) than the uncoated zinc and the values were the nearly identical. Therefore, it can be concluded that the PLLA coating was stable in 1-14 days and provided an effective barrier to corrosion for the Zn substrate. Also, it can be seen that the 1 and 3 µm PLLA coatings have essentially the same behavior in protecting the Zn surface from corrosion.

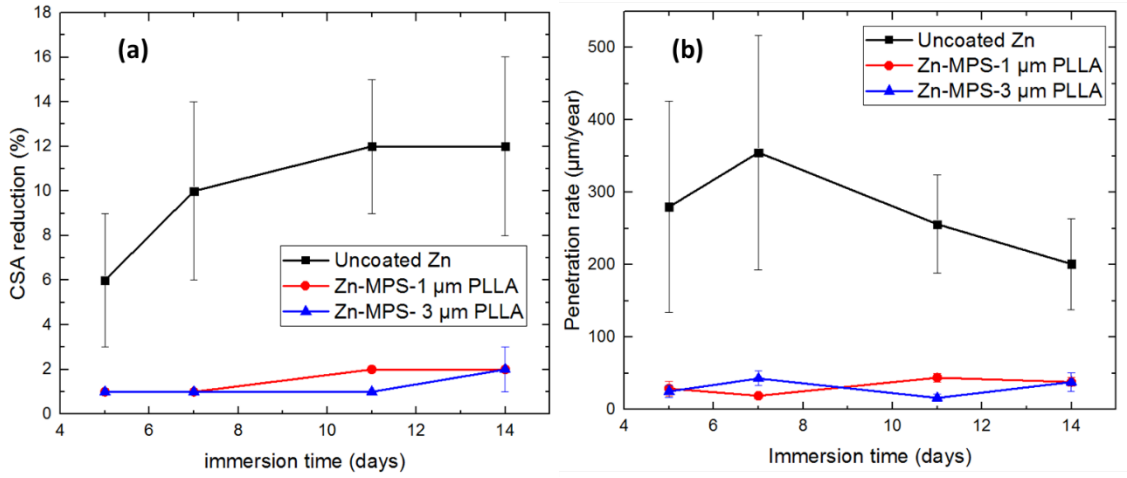

Figure 6.6. Measured a) CSA reduction and b) PR of the uncoated Zn and modified Zn PLLA coated wires after different exposure times to SBF.

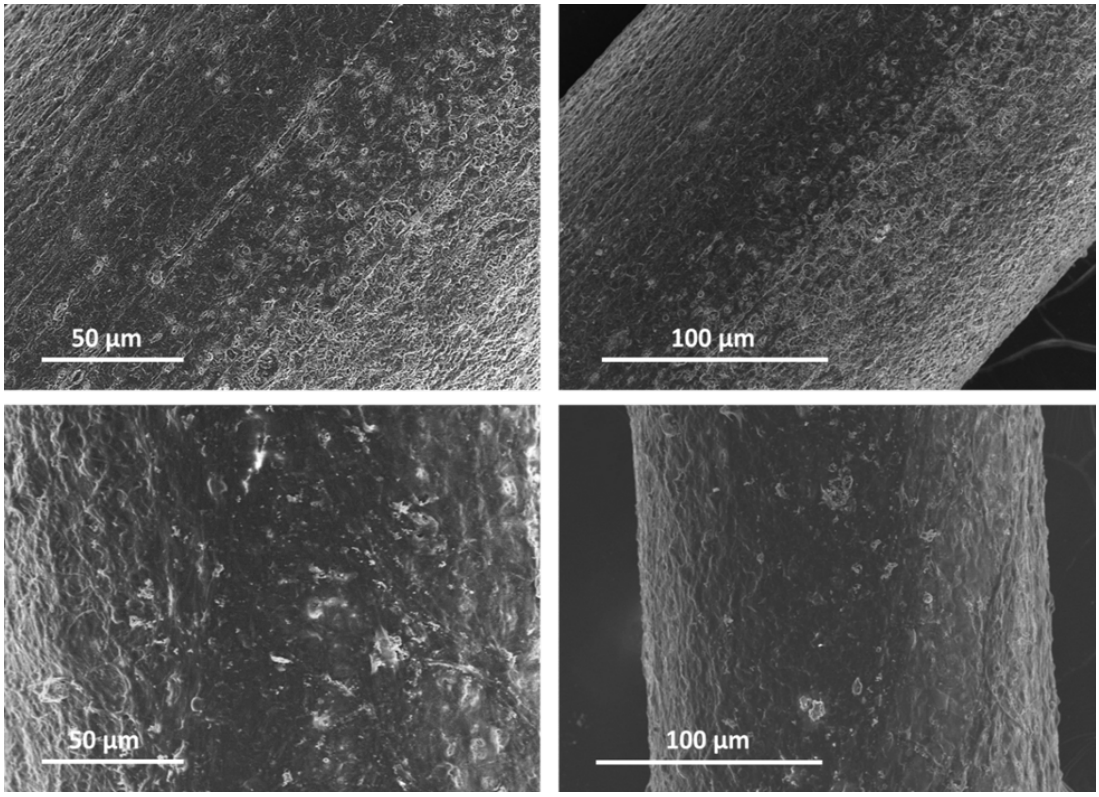

Figure 6.7. FESEM of the PLLA coated wires with a, b) 1µm and c, d)3 µm PLLA coating after immersed in SBF for 14 days.

The FESEM images of the surface of the PLLA coated samples after incubation in SBF at 14 days are shown in figure 6.7. The surface images of the MPS modified PLLA coated Zn wires illustrate the presence of the polymer coating and reflect solid adhesion of the polymer to the Zn substrate in SBF for 14 days. However, initial swelling and delamination of the coating are noticeable.

Formation of gas bubbles on the surface of the PLGA coated Mg4Y and AZ31 magnesium alloys which were observed on the 12 days incubated specimens by Ostrowski *et al*. [36]. No evolution of gas was observed for the PLLA-coated Zn wires. This can be due to the difference in the degradation behavior of Zn and Mg. Mg degradation in a chloride containing solution such as SBF leads to the formation of hydrogen gas evolution and gas pocket formation [36]. The hydrogen gas bubbles which are trapped underneath the coating finally burst and appears as the plate-like morphology on the surface of the Mg substrate

[36]. This morphology which is typical for the magnesium corrosion products was not observed on the Zn substrate. Instead, the formation of local cracks and polymer coating peeling were observed (figure 6.7).

6.2.2 Electrochemical tests

6.2.2.1 Potentiodynamic polarization

MPS modified Zn substrate was coated with 1 μm of PLLA on the modified Zn wires as described earlier. The wires were used directly for the test and SBF was used as the electrolyte. After reaching a stable open circuit potential, the polarization test started at a scan rate of 1 mV/S. The corrosion potential could be read from the polarization curve where the anodic and cathodic curves intersect. Then the corrosion current could be determined by intersecting the Tafel extrapolation on the anodic curve with the corrosion potential. Origin software was used to extrapolate the Tafel line and to plot the data. Figure 6.8 illustrates the polarization curves for the uncoated and coated Zn substrates. A summary of the measured corrosion potential and corrosion current densities as calculated from Tafel extrapolation are presented in table 6.3. Corrosion rate could also be calculated with equation 4 in chapter 5.

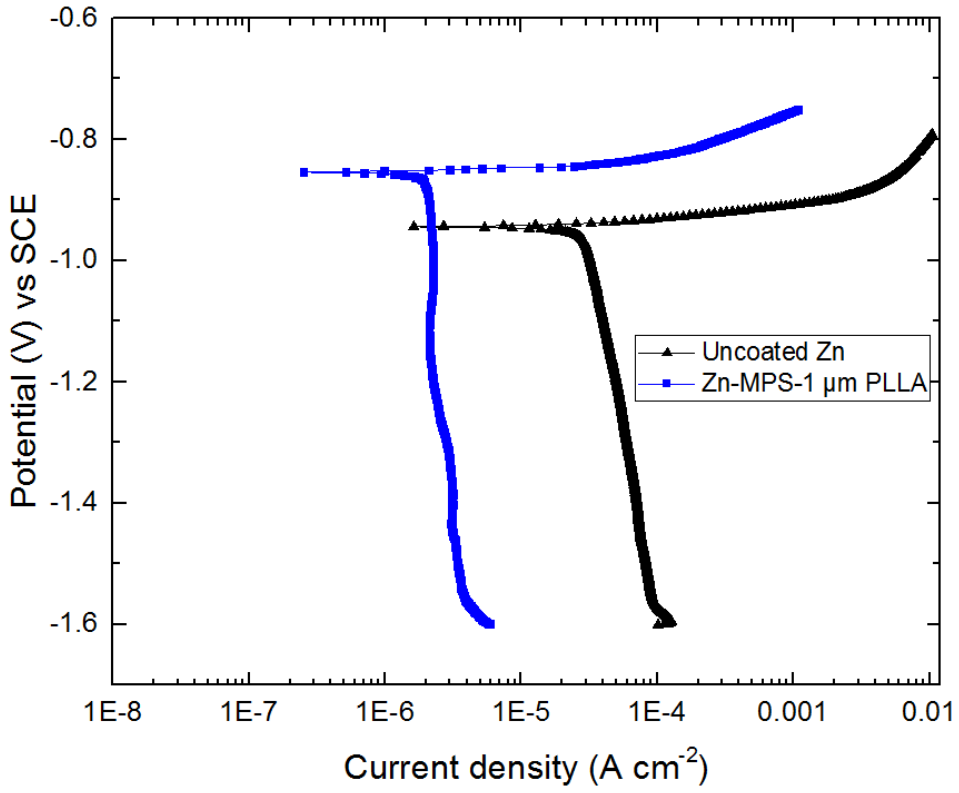

Figure 6.8. Potentiodynamic curves of uncoated and PLLA coated wires with two different thicknesses after being immersed in SBF

The E_{corr} value of the uncoated Zn is higher than the E_{corr} of the MPS modified 1 µm PLLA coated Zn substrate which indicates that the coated substrate is less prone to corrosion. The i_{corr} value for the coated sample is also much lower than the bare Zn substrate by approximately one orders of magnitude. The cathodic curve for the uncoated and coated Zn is flattened which suggests that the cathodic reaction is under diffusion control (concentration polarization) and there is a diffusion problem for oxygen species (Figure 6.8). When the O_2 cannot reach the surface, the polarization curve data becomes extremely asymmetric, and as a result, there is a reduction in the corrosion rate. Concentration polarization leads to a limiting current in the cathodic site of the reaction. We cannot surpass this current with increases in the potential. One technique to study whether or not there is concentration polarization is the rotating disc electrode. Since we did not have access to this technique, the potentiodynamic polarization test was repeated under two

conditions: increasing the stirring rate of the electrolyte (three times higher) and with no stirring condition. This method allows us to observe any issues with diffusion. If the corrosion current changes as the stirring speed changes, then we can conclude that we have concentration polarization. The same flattened cathodic curve and higher i_{corr} was obtained by changing the stirring speed. Thus, we concluded that concentration polarization exists for both the coated and uncoated substrate. The concentration polarization might be due to the geometry of the working electrodes that we are using (wires). In this situation, the corrosion rate is, in fact, equal to the limiting current density.

Table 6.3 Calculated corrosion potential, corrosion current density and corrosion rate from polarization test.

Substrate	$\mathbf{E}_{corr}$ vs SCE (mV)	$\mathbf{i}_{Corr}$ (μA cm^{-2})	**Corrosion rate (mm/year)**	**Corrosion rate (μm/year)**
Uncoated Zn	-944.35	20	0.29	290
Zn-MPS-1 μm PLLA	-841.22	2	0.03	30

The calculated mean value of the corrosion rate of the uncoated and 1 μm PLLA coated specimens from the immersion test are 273 and 33 μm/year, respectively. These values are fairly similar to the calculated values from the potentiodynamic polarization test.

Another way to ensure that the calculated current density is current is to do EIS and measure the polarization resistance of the specimens, and then substitute the values in the following equation [82].

$$i_{corr} = \frac{1}{2.303Rp\,(\frac{1}{ba}+\frac{1}{|bc|})} \quad (13)$$

In which R_p is the polarization resistance and b_a and b_c are the anodic and cathodic Tafel slopes, respectively. The cathodic Tafel slope is almost infinite, therefore $\frac{1}{bc}$ approaches zero. By substituting b_a as 0.018 and Rp as 6000 Ωcm^{-2}, calculations will be shown in the next subsection, we can get i_{corr} for the coated Zn as 2 μA cm^{-2}. This value is exactly equal to the value which was read off of the graph from the limiting current. Therefore, we can conclude that the obtained i_{corr} values are correct.

6.2.2.2 EIS

The EIS test was performed on two polymer coated specimens with two different thicknesses and on the uncoated substrate to investigate the effect of the modification and polymer coating on the polarization resistance and impedance of the specimens. Figure 6.9 represents the obtained Nyquist (Fig. 6.9a) and Bode (Fig 6.9b) plots for the two coating specimens and the uncoated specimens. The frequency varied between 100 kHz to 0.1 Hz.

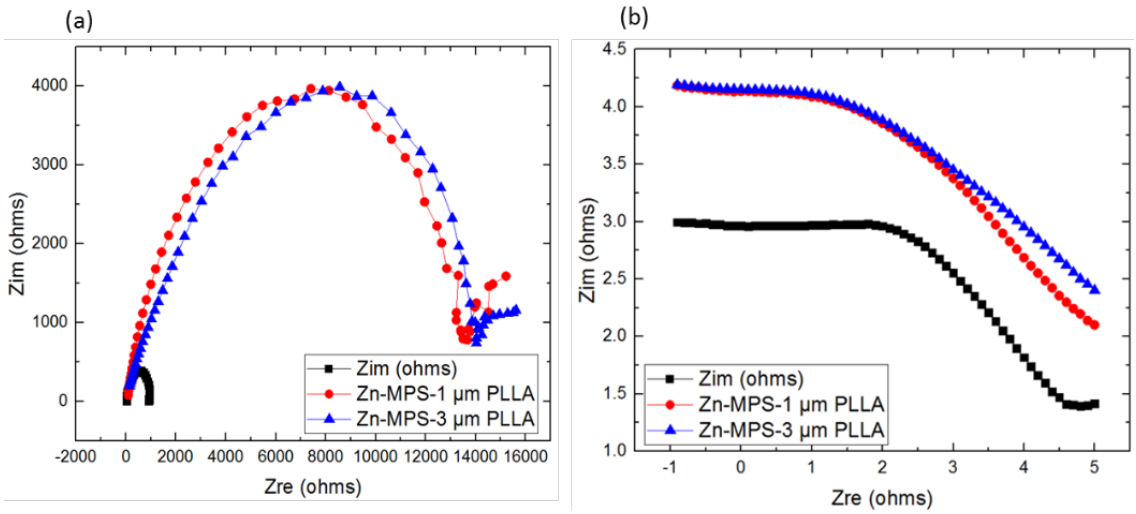

Figure 6.9. EIS plots of the coated and uncoated samples.

As it can be seen in figure 6.9a, the uncoated sample represents a much lower Zre (real part of the impedance) value, which is an indicative of the polarization resistance of the specimen, compared to the coated samples. Large polarization resistance is a characteristic for a good barrier coating on the Zn substrate. The upward trend which appears in the far right of the X-axis of the Nyquist plot of the coated specimens at low frequencies are indicative of the concentration polarization which shows that the coating is serving as "kinetic barrier" to corrosion reaction at the surface and it is slowing the diffusion of the electrolyte to the surface. However, the uncoated Zn sample does not show any evidence of polarization at low frequencies. Also, the coated specimens with two different thicknesses show similar behavior in protecting the surface as it was shown earlier by the immersion test. The impedance of the coated and uncoated specimens can be compared by

Bode plot (figure 6.9b). It presents changes in impedance values after polymer coating deposition. Table 6.4 shows the comparison between the impedance and polarization resistance of the uncoated and modified coated Zn substrate at low frequency (0.1 Hz). The impedance value for the uncoated Zn wire at low frequency is 912 ohms cm^2 whereas, for the 1 and 3 μm PLLA coated specimens is 15300 and 15661, respectively, approximately 16 times higher than of the uncoated substrate. The higher impedance value indicates significant protective barrier property of the coating.

Table 6.4. Polarization resistance and impedance of the uncoated and coated substrates

Substrate	Polarization resistance (ohms cm^2)	Impedance (ohms cm^2)
Uncoated Zn	912	985
Zn-MPS-1 μm PLLA	15215	15300
Zn-MPS-3 μm PLLA	15618	15661

Therefore, it can be concluded that the MPS modification and PLLA coating have a significant influence on increasing the polarization resistance and impedance of the Zn surface and therefore decreasing the corrosion rate of the metal.

The MPS modified 1 μm PLLA coated Zn wires were immersed in SBF solution at 37ºC at 5 different time points (i.e. 3, 5, and 10 days) in order to check the stability and effectiveness of the coating after being exposed to a corrosive environment. Figure 6.10 illustrates the EIS results of the MPS modified 1 μm PLLA coated specimens exposed to SBF at various time points. The frequency varied from 100 kHz to 1 Hz.

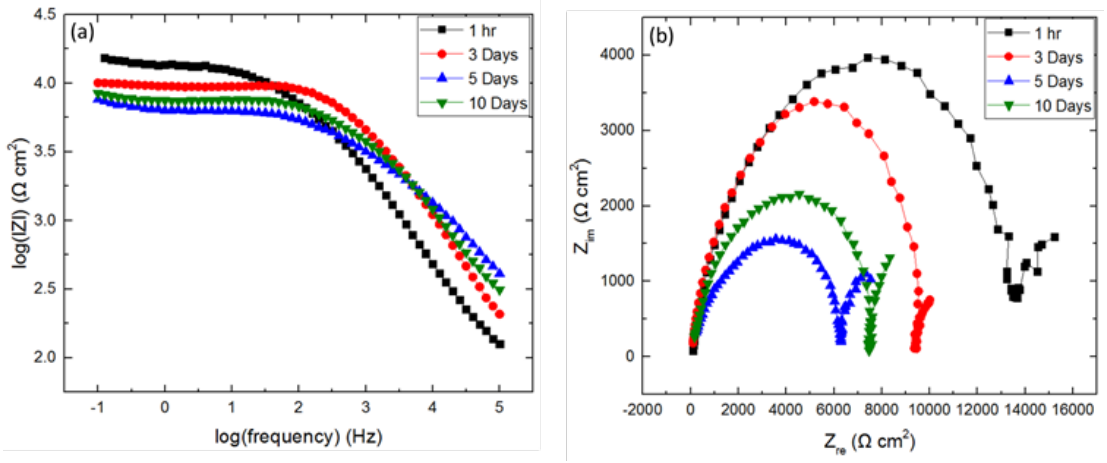

Figure 6.10. EIS results of MPS modified PLLA coating on Zn after various exposure times in SBF.

The Bode plot (Figure 6.10a) represents changes in impedance during 10 days of immersion in SBF. The systematic changes in the Bode plots support the view that electrolytes penetrate the PLLA coating during the 10 day immersion period. After 3 and 5 days, minor changes in the impedance may be due to the penetration of ions from the electrolyte to the surface of the metal. The increase in the impedance after 10 days of immersion in SBF can also be seen in comparison to the 5 day immersion, which may be due to the precipitation of calcium phosphate on the surface of the wire or water penetration into the PLLA coating. Indeed, sample imaging under SEM and EDS analysis revealed the presence of elemental calcium and phosphate on the PLLA coating surface. EDS analysis was performed on the 10 days immersed specimen in SBF to investigate the present elements on the surface. The result of the EDS analysis is presented in figure 6.11. Fairly intense peaks were observed for the calcium and phosphate elements. Thus, the increase in the impedance may be because of the existence of the calcium-phosphate layer on the polymer coating

The lZl value at the low-frequency region decreased from approximately 15300 Ωcm2 to 8320 Ωcm2 for these two samples (Figure 6.10a), which is eight times higher than the initial impedance of the uncoated Zn substrate.

The decrease in impedance shown in Figure 4 implies the penetration of electrolyte into the coating and exposure of the Zn surface to the electrolytes; this contact of metal with electrolytes initiates corrosion. The effect of the sample exposure to SBF over time can also be analyzed on Nyquist plots, as shown in Figure 4b. A reduction in the diameter of plots during 10 days exposure is indicative of a decrease in the PLLA-coated specimen corrosion resistance. This is likely to have occurred because the ester linkage of PLLA is destroyed by hydrolysis in the surrounding physiological environment at 37 ºC.

As shown in Figure 6.10b, the Nyquist plots remain as concave-shaped curves over the entire sequence of experimentation. This suggests the coating maintains its protective physical barrier function even after 10 days of contact with the electrolyte solution. The corrosion resistance properties are in fact a combination of both PLLA and silane coupling agent. PLLA swells in electrolyte solutions and hydrolysis takes place at the beginning of PLLA contact with SBF. Previous studies indicate that the amorphous portion of PLLA degrades ahead of the crystalline structure, and the molecular weight of the polymer decreases as a result of polymer hydrolysis of their hydrolysable bonds and formation of oligomers and monomers.

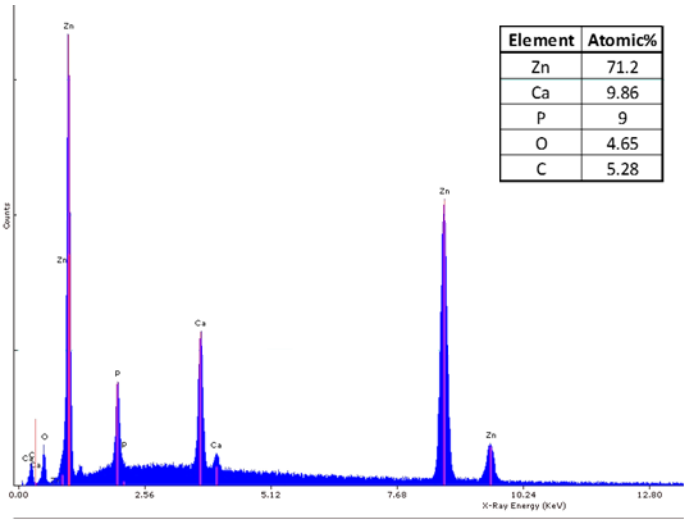

Figure 6.11. EDS spectrum of PLLA coated Zn after immersed in SBF for 10 days.

6.2.3 ICP

The ICP test was performed over 14 days' immersion in SBF to monitor the release of the Zn^{2+} and Ca^{2+} of the uncoated and coated specimens into the solution. The correlation between the Zn and Ca ions release into the solution and immersion time is represented in figure 6.12.

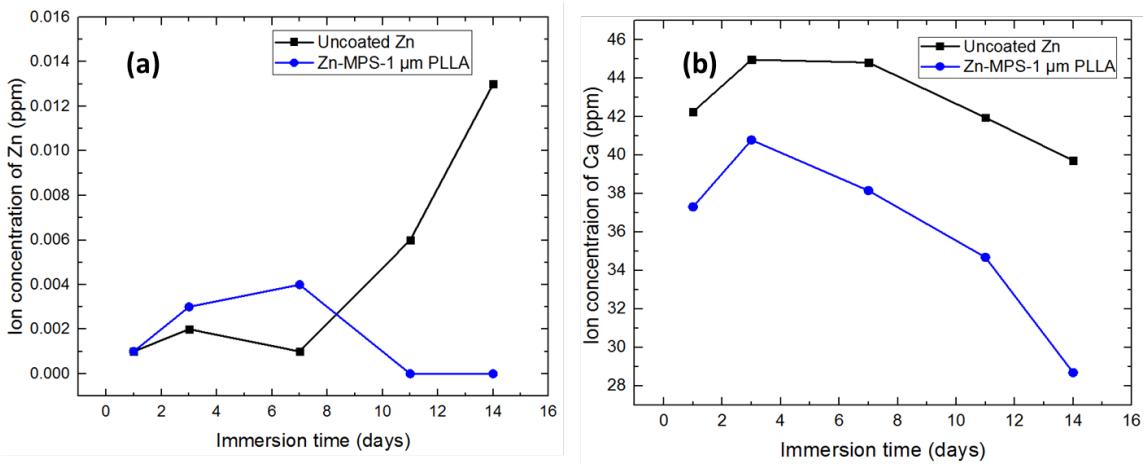

Figure 6.12. Ionic concentration of Zn, Ca and P in SBF over different immersion time of coated and uncoated specimens.

The Zn ion concentration increased from approximately 0.003 ppm after one day of immersion in SBF to 0.013 ppm after 14 days of immersion. The release of Zn ions to the solution has increased approximately four-fold during the 14 days' immersion in SBF, while the release of the Zn ion for the coated specimens had less variation during the 14 days' time point. The ionic concentration of Zn has increased slightly from 0.001 to 0.004 ppm over 7 days of immersion in SBF. However, the coated substrate shows some reduction in Zn ion release after 7 days of exposure to SBF, and no release of Zn ion was observed between 11 to 14 days of immersion. Therefore, the reduction in the release of the Zn ions to the SBF was observed by coating the substrate. This demonstrates the effectiveness of the coating in providing a barrier between the metal surface and the electrolyte to be an obstacle for ion dissolution and to hinder the release of Zn ions from

the metal to the solution. The decrease in the Ca ionic concentrations was observed for both the uncoated and coated specimens after 3 days of SBF immersion. The SBF solution is itself supersaturated with apatite. The decrease of Ca^{2+} might be due to the deposition of an apatite layer on the surface of the wires. Also, the ionic concentration of Ca^{2+} for the PLLA coated wires is much lower than the uncoated Zn wires.

6.3 *In vivo* test results

6.3.1 Corrosion analysis

After explanting the wires, the in vivo corroded wires were mounted in epoxy, cross-sectioned and then imaged by the procedure explained in subsection 5.3.1.1.1. The portion of the wire which remained in the artery for two weeks did not have any tissue attached to it, so a small portion of the wire was cut and the surface was investigated by SEM (Figure 6.13).

.

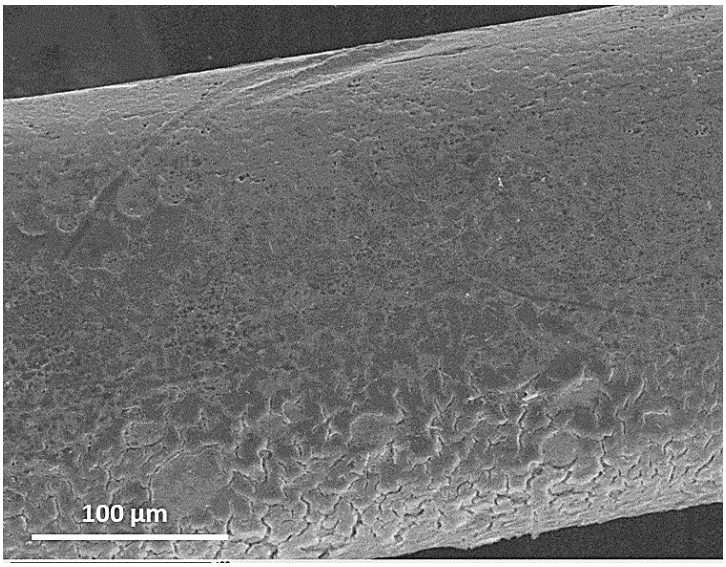

Figure 6.13. Surface of the *in vivo* corroded wire after two weeks.

The presence of the PLLA on the wire can be seen clearly in figure 6.13. After two weeks of implantation, the polymer coating still exists on the Zn substrate without showing any sign of swelling, delamination or being peeled off from the substrate. However, initiation of cracks formation is noticeable. PLLA is a brittle polymer thus, appearing flaws and

defects such as cracks which are related to the brittle nature of a material is not unexpected. Also by comparing the Figure 6.13 with figure 6.7a, b more surface cracks were observed in the rat implantation study. However, this level of cracking was not observed in the *in vitro* study. A potential cause of this is that the wires were damaged during the implantation phase because the wires were handled and inserted with tweezers during the rat study but not during the *in vitro* immersion test study. Since PLLA is a brittle polymer applying force on the PLLA coated wires for inserting them into the artery can cause the cracks.

The representative back scattered images of the *in vivo* corroded 1µm PLLA coated MPS modified Zn wires which remained in the abdominal aorta of Spraque-Dawley rats for 0.5, 3, 4.5, and 6 months are presented in figure 6.14.

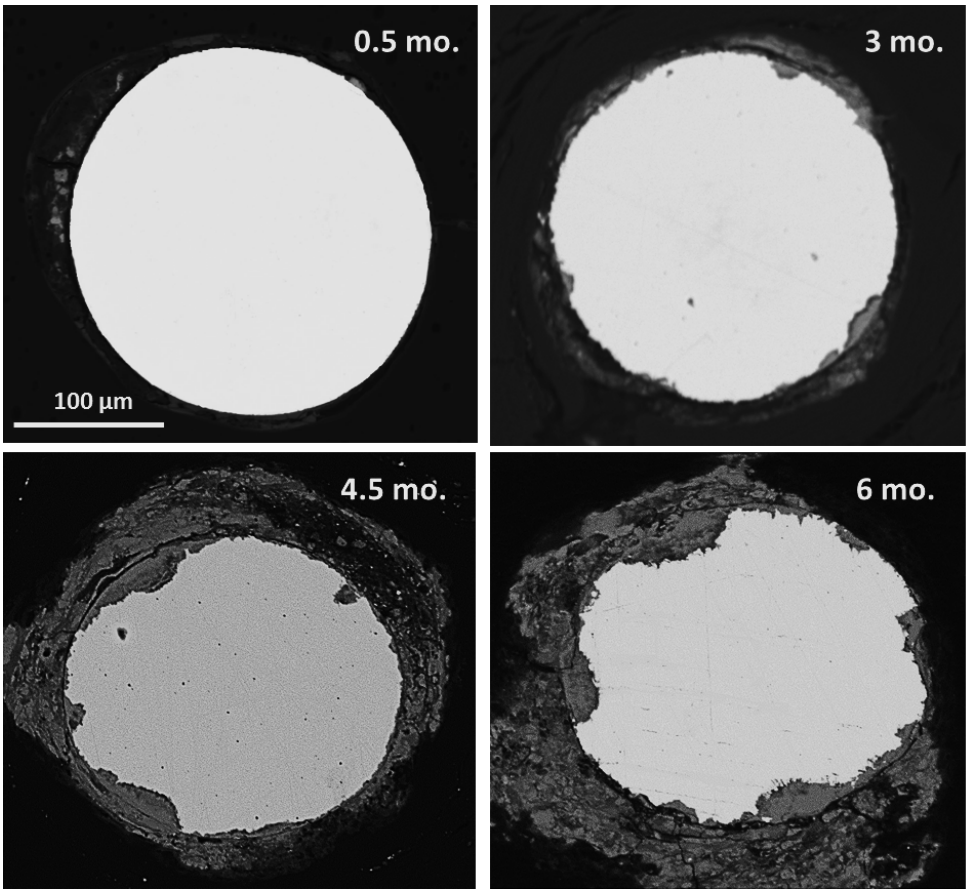

Figure 6.14. Representative BSE images of the *in vivo* corroded PLLA coated wires after different time points.

The number of cross sections which were used for calculating the CSA% reduction and PR were 12 to 15 for each wire. The mean percent of CSA reduction and penetration rate was calculated and are shown in figure 6.15. The error bars are also represented in this figure which shows the standard error. Quantitative evaluation of the PLLA coated wires was necessary for comparison with the values which was reported elsewhere [11] for the uncoated Zn wires corroded *in vivo* for 1.5, 3, 4 and 6 months.

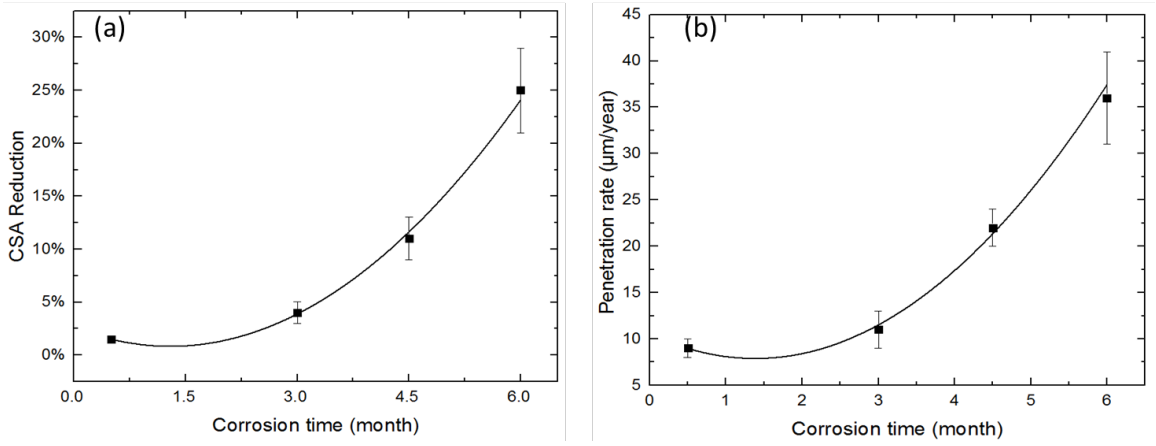

Figure 6.15. Calculated CSA reduction and PR for the in vivo corroded PLLA coated Zn wires.

For both the CSA% reduction and PR data the polynomial regression best fits the given sets of data points (R^2=0.99 and 0.98 for CSA% and PR, respectively), suggesting a non-linear trend for reduction in the cross-sectional area and penetration rate of Zn ions overtime. In figure 6.15(a) it can be observed that the cross-sectional area is being reduced at an exponential rate which can be interpreted as the increment in corrosion rate. Note that between zero and 4.5 months the CSA% reduction is minimal, meaning the polymer is essentially stable during this timeframe and the CSA% reduction remains under 11% up to 4.5 months. The exponential relationship is observed dramatically between 4.5 and 6 months as the CSA% reduction moved from 11 to 25% which implies the acceleration in degradation of the polymer coating and complete penetration of the electrolyte into the Zn substrate. However, after 6 months the PLLA coated wire maintained 75% of its initial

sectional area which means that it can maintain its mechanical stability for 6 months, allowing for the completion of the healing process, and thereafter disappearing quickly.

According to figure 6.15(b) After 4.5 months a drastic increment in penetration rate can be observed which can be due to the degradation of the polymer coating and exposing the zinc substrate to the physiological environment.

The observed *in vivo* corrosion behavior of the MPS modified 1 µm PLLA Zn wire was compared with the observation of the uncoated Zn wire reported by Bowen *et al.*[11]. The comparison between the measured CSA% reduction and PR for the uncoated and MPS modified 1 µm PLLA coating at 3, 4.5 and 6 months is illustrated in figure 6.16. The CSA% reduction and PR of the uncoated Zn and MPS modified PLLA coated Zn wires are modeled by a second order (n=2) polynomial regression.

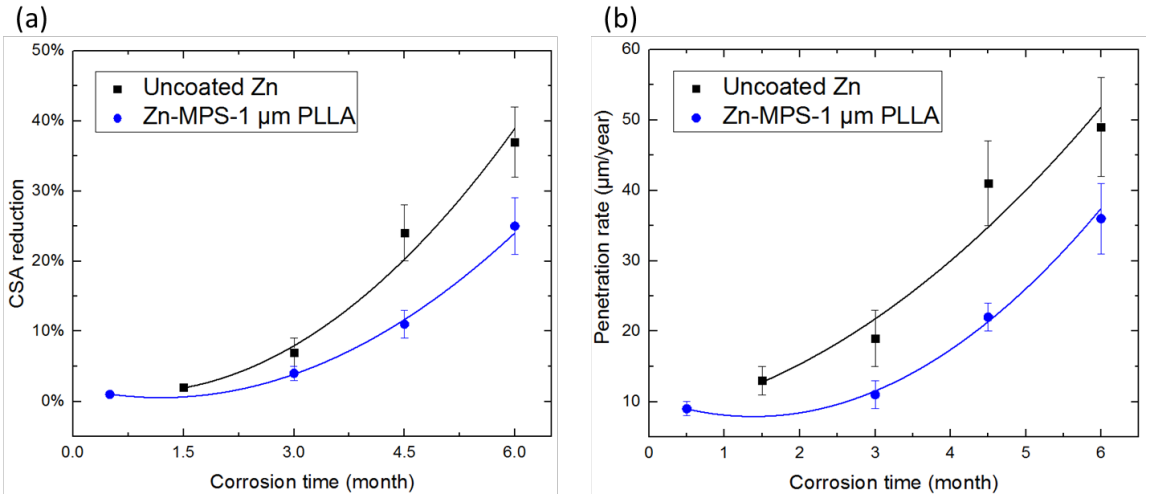

Figure 6.16. Comparison between a) CSA reduction and b) PR of the uncoated Zn and MPS modified PLLA coated Zn wires corroded *in vivo* 3 to 6 months. Error bars are not shown for clarity.

Significant reduction in the penetration rate and cross-sectional area reduction of the polymer treated wires, which can be observed in figure 6.16, are indicative of the significant influence of modification and polymer coating on Zn substrate on the corrosion properties of Zn. Up to 4.5 months the penetration rate of the PLLA coated wire is 22

μm/year which is approximately close to the 20 μm/year necessary design criterion for bioabsorbable stents [86]. Therefore, by modification and applying the polymer coating we approach the ideal degradation benchmark for bioabsorbable stents. An acceleration in biocorrosion of the polymer coated specimens can also be observed after 4.5 months of implantation due to the noticeable increase in CSA reduction from 11 to 25%. However, this accelerated increase for uncoated Zn was observed after 3 months of implantation [11].

The present corrosion products on the cross section of the PLLA coated wire which spent 3, 4.5 and 6 months in the abdominal aorta of rats was investigated by ESEM and EDS and is presented in figure 6.17.

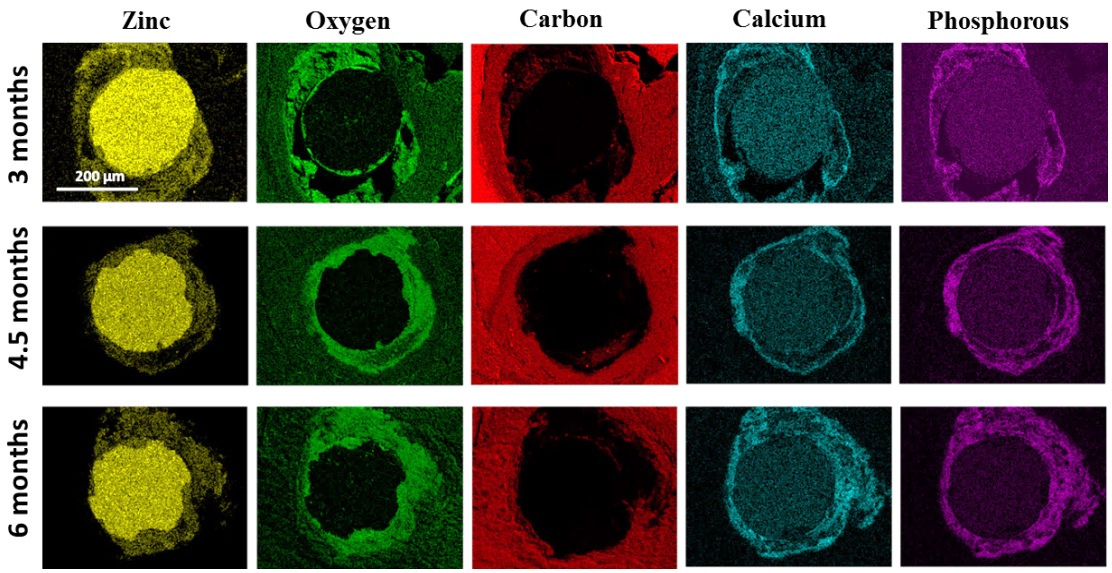

Figure 6.17. Representative individual elemental maps of the cross sections of the 3, 4.5 and 6 months explanted wires presented in figure 6.14.

At 3 months a thin layer of zinc oxide is the dominant corrosion product. No significant presence of the other elements such as carbon, calcium, and phosphorous were observed. At 4.5 and 6 months the oxygen layer is thickened and the presence of phosphorous and calcium around the cross section is more noticeable in comparison to the three months' explant. Carbon does not appear to be a substantial corrosion product since no significant layer can be seen around the cross section of the wire. The obtained results can be compared

with the reported corrosion products on the 4.5 months *in vivo* corroded bare Zn wire by Bowen *et al* [11]. For the bare Zn at 4.5 months, Zn carbonate is the dominant corrosion layer, which surrounds the metallic Zn cross section, and the Zn oxide is dispersed throughout the Zn carbonate layer. Zn oxide is also separated by the Zn carbonate.

To investigate the influence of the polymer thickness on the corrosion resistance of Zn wires two other specimens with the thickness of 3 and 12 μm were prepared by the procedure described in subsection 5.1.3. The thicker polymer coating can be obtained by increasing either the concentration of PLLA in DCM or increasing the withdrawal velocity of the wire from the solution or both (which was the situation for 12 μm coating). The specimens with thicker polymer coating were implanted in the abdominal aorta of rats for two weeks. After explanting parts of the wires which tissue was not adhered to them was cut and cleaned with ethanol. After carbon coating the wires, FESEM was used to investigate the morphology of the surface of wires after two weeks' time *in vivo* test (figure 6.18).

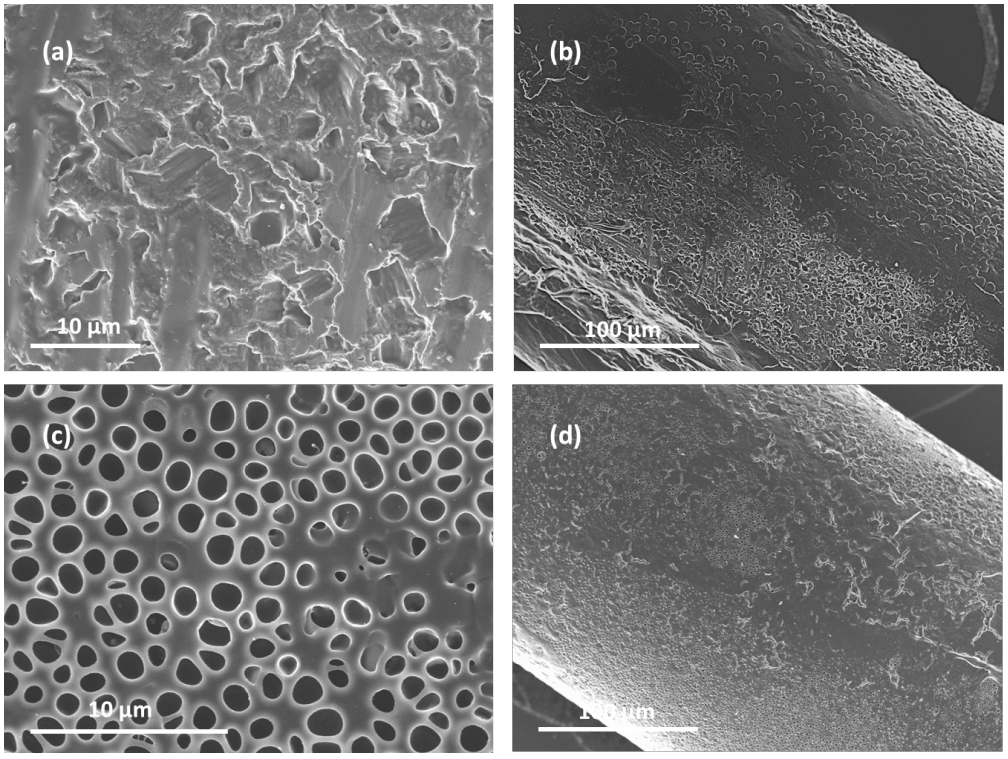

Figure 6.18. SEM images of the surface of the PLLA coated wires after two weeks' time in vivo. a, b represents the 3 µm PLLA coating and c, d represent the 12 µm PLLA coating.

Electron microscopic inspections indicate that the PLLA coating exists on the Zn wire after two weeks. The porous surface structure of the 12 µm PLLA coated wire could still be observed after explantation. However, deformations and delamination of the PLLA coating were observed on the surface of the wire. The surface morphology of the thicker polymer coatings can be compared with the thin polymer coating which was reported earlier (figure 6.13). Swelling, delamination and damage in the polymer coating can be seen in the 3 and 12 µm PLLA coating which was not observed in the 1 µm PLLA coating. Also, the 12 µm PLLA coating is still maintaining its porous structure which was shown earlier before implantation (figure 6.4c).

The degradation rate of the wires was evaluated by measuring the CSA% reduction and penetration rate of the explanted wires and then were compared to the 1 µm PLLA coated wire which was initially studied. The representative cross sections of the explanted wires are represented in figure 6.19.

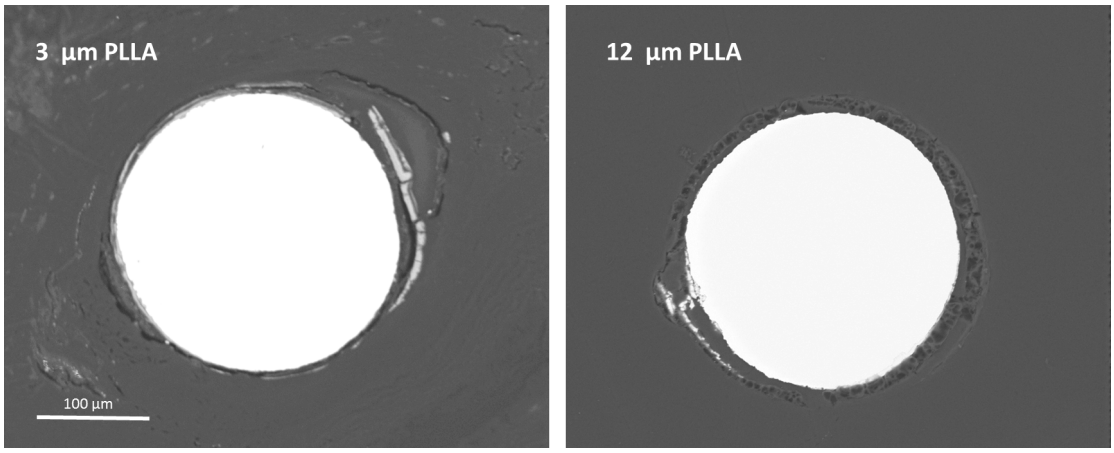

Figure 6.19. Representative BSE images of the *in vivo* corroded wires after two weeks with two different thicknesses.

The polymer coating can be seen clearly around the cross section with 12 µm PLLA coating in figure 6.18 but the coating is less obvious in 3 µm PLLA coating. The cross section was used to confirm the deposited thickness of the coating by measuring the area around the polymer coating (A2) and the area around the bright zinc wire (A1) (Figure 6.20). By measuring the areas, the radius of both circles could be measured. By subtracting the correspondent radius to A1 from the correspondent radius to A2 the thickness of PLLA could be measured which was 12 µm as it was reported earlier.

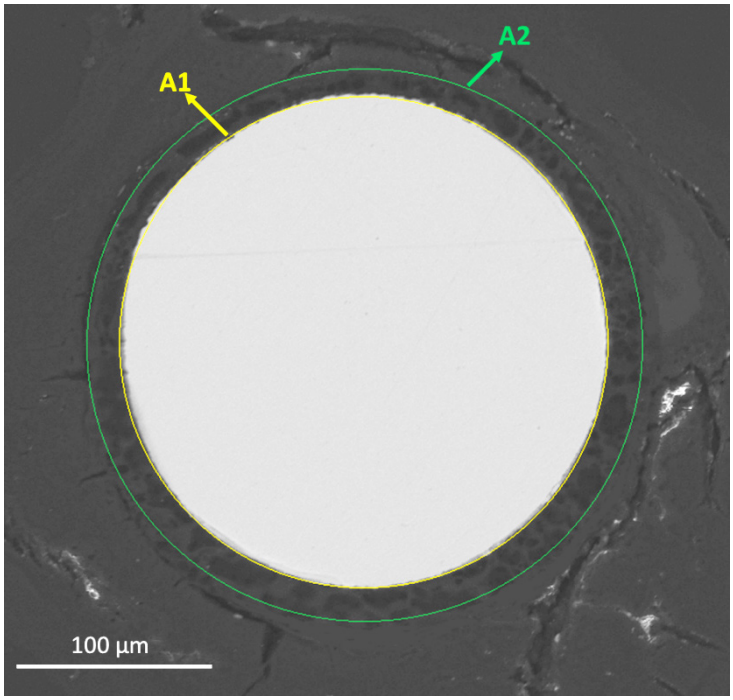

Figure 6.20. Second method for measuring the thickness of PLLA around Zn wire.

The calculated average CSA% reduction and PR for the 3 and 12 µm PLLA coatings are presented in table 6.5. The calculated values for 1 µm PLLA in the previous experiment is also presented for a better comparison between the three different thicknesses of PLLA.

Table 6.5. PR and CSA% reduction for different polymer thicknesses after two weeks of *in vivo* test

Polymer thickness (µm)	**Corrosion Time (mo.)**	**Penetration Rate ± Standard error (µm/yr)**	**CSA Reduction ± Standard error (%)**
1	0.5	9 ± 1	0.5 ± 0.1
3	0.5	8 ± 2	0.4 ± 0.2
12	0.5	6 ± 2	0.4 ± 0.1

Increasing the thickness of the polymer coating did not have any significant influence on the reduction of the cross-sectional area. The penetration rate has reduced from 9 µm/year to 6 µm/year by depositing 12 times thicker polymer coating. However, the obtained results of the protection behavior and barrier properties for the thick and thin polymer coating are

pretty much the same. No significant difference was obtained by applying a thick polymer coating. This is because surface cracks appear due to the brittle nature of PLLA when the coating degrades. Regardless of thickness, the corrosive medium can penetrate through to the metal surface as the result of the break down in the polymer coating.

6.3.2 Biocompatibility and toxicity

The corrosion rate of PLLA coated Zn substrate matches the ideal bioabsorbable corrosion rate, as discussed earlier. However, the biocompatibility needs to be investigated further due to the unknown toxicity of the PLLA coating on the zinc substrate. Uncoated 4N-Zn *in vivo* degradation has shown a favorable host response [12]. Hence, the effect of the polymer coating on Zn biocompatibility was investigated. Figure 6.21 represent the obtained H&E stained images of the wires after residence in the abdominal aorta of rats for 0.5, 4, 4.5 and 6 months.

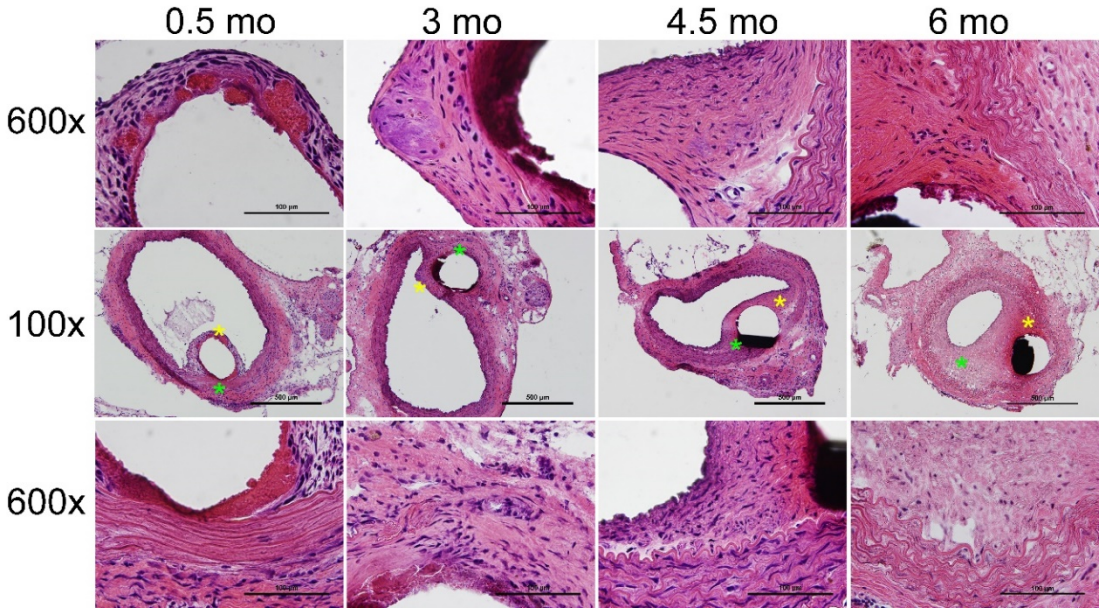

Figure 6.21. Low magnification and high magnification images (middle and flanking rows respectively) of the entire artery and regions of interest (yellow asterisk corresponds to top row; green asterisk corresponds to the bottom row) shown by H&E staining of histological cross-sections. Cell nuclei are purple and surrounding tissue, matrix, muscle etc. are various shades of red-pink.

At two weeks we observe toxicity in the neointimal tissue at the interface between the tissue and the wire. Smooth muscle cell death occurred at the two-week mark in the media layer as shown by the green asterisk and seen at high magnification directly below. At the three-month mark, toxicity can be observed in the surrounding neo-intima, shown by the green asterisk. At 4.5 months we see a slight reduction in toxicity but an increase of intima thickening in comparison to the 3 month mark. It appears to be spreading throughout the artery and the response is propagating throughout the vessel (high mag panel referring to green asterisk). At six months, a large neo-intima has developed and has narrowed the original lumen of the artery significantly. Therefore, the progression of the response from 2 weeks to 6 months generally worsens. To be clear, up to 3 months the conditions are stable, but after that time the conditions steadily worsen. However, the obtained results belong to one specimen per time point and are the observations for a single specimen, meaning this is not extremely conclusive. This finding are reported as a general observation with the implantation of these wires. There remains a need to repeat the implementation at a higher sample size if there want to be a continuity in this type of modification.

The released of toxic and acidic by-products of PLLA degradation such as initiators, catalysts, and solvents in addition to its main corrosion products, which can be metabolized and removed from the body easily, can be the main reason for reducing its biocompatibility [60]. Provoking a negative inflammatory and foreign body responses and toxicity in the cellular environment surrounding the PLLA implants were reported before [87-90]. Although the induced injuries are not major and they are not very irritable to the cell, they should be reconsidered for being used as fully biocompatible materials for clinical applications.

7 Conclusion

In this study, a polymeric coating of poly (L-Lactic-acid) (PLLA) was applied to metallic zinc (Zn) implant material in an effort to delay and manipulate the degradation rate of Zn in the endovascular environment. The surface of Zn was modified with 3-(trimethoxysilyl) propyl methacrylate (MPS) to increase the adhesion between the metallic substrate and the

polymer coating. Homogeneous and smooth PLLA coatings with a thickness of 1 to 12 μm was deposited on the surface of the modified Zn wires by a dip coating method. Immersion tests in the simulated body fluid (SBF) solution, electrochemical analysis, ICP and microscopic observations were used to investigate the *in vitro* degradation rate of the modified and PLLA coated specimens and compared with the results for the bare Zn substrate.

The experimental penetration rates and cross-sectional area reductions for the MPS-modified PLLA coated wires were approximately 5 times smaller than for uncoated Zn substrate after 14 days' immersion in SBF. Electrochemical impedance spectroscopy (EIS) was used to compare the impedance and polarization resistance of the uncoated and coated specimens and to evaluate the polymer coating performance after long-term exposure to SBF. Remarkable enhancements in the polarization resistance and impedance (16 times higher) of the modified and coated specimens were observed. Furthermore, evidence of concentration polarization could also be observed on the polymer coated samples. However, after exposure of the specimens to SBF solution, reductions in the impedance and polarization resistance of the specimens were recorded, which imply initiation of the destruction of the polymer coating and penetration of the electrolyte to the Zn substrate. Although the impedance and polarization resistance of the polymer coated wires decreased after 10 days' immersion in SBF solution, the impedance and polarization resistance values were still higher than for the bare Zn substrate. Potentiodynamic polarization test was also showed a less negative corrosion potential and 20 times lower value of corrosion current density for the modified 1 μm PLLA coated Zn in comparison to the uncoated Zn. The ICP test also demonstrated a slower release rate of Zn^{2+} to SBF for the 1 μm PLLA coated sample in comparison to the uncoated Zn over 14 days' immersion in SBF which indicates an effective barrier to the ion transformation was provided by a polymer coating.

Electron microscope investigations were also carried out to evaluate the surface of the polymer coated wires after immersion in SBF solution. It was observed that after 14 days of exposure to SBF the polymer coating was intact on the surface of the Zn wires, with

only local cracking. No evidence of swelling, delamination or destruction in the polymer coating was observed.

The *in vivo* study involving implantation of Zn-based implants into abdominal aorta of rats also indicated a reduction in the corrosion rate of the MPS-modified PLLA coated Zn substrates. The cross-sectional area reduction dropped from about 37% for the bare Zn substrate to about 25% for the PLLA coated samples at 6 months' implantation time. The penetration rate of the Zn ions was also reduced from about 49 μm/year to 36 μm/year for the PLLA coated wires. Also, no significant difference in the corrosion behavior by applying a thicker polymer coating could be observed.

Biocompatibility and cytotoxicity of the PLLA coated wires and their potential for cardiovascular stent application and drug-eluting systems were investigated. Our studies indicated reduced cell biocompatibility, with toxicity around neointima after three-month residency in the abdominal aorta of rats. Besides toxicity, the luminal cross-sectional area was considerably reduced from 4.5 to 6 months causing obstruction to the blood flow.

In conclusion, MPS modification and PLLA coating on the metallic Zn substrate increase the corrosion resistance and reduction of the biocorrosion rate of the implants in the first few months. However, the reduction in biocompatibility of the PLLA-coated Zn implants highlights a challenge for bioabsorbable stents application that needs to be addressed in the future.

8 References

[1] Stewart J. Technology in interventional cardiology: Percutaneous transluminal coronary angioplasty. Journal of medical engineering & technology 1991;15:99-106.
[2] Moravej M, Mantovani D. Biodegradable metals for cardiovascular stent application: interests and new opportunities. Int J Mol Sci 2011;12:4250-70.
[3] Fan WJ, D; Feldman, M. Metallic Stents Coated With Bioabsorbable Polymers. Cardiac Interventions Today:42-9.
[4] Ormiston JA, Serruys PW. Bioabsorbable coronary stents. Circ Cardiovasc Interv 2009;2:255-60.
[5] Erne P, Schier M, Resink TJ. The road to bioabsorbable stents: reaching clinical reality? Cardiovasc Intervent Radiol 2006;29:11-6.

[6] Waksman R. Promise and challenges of bioabsorbable stents. Catheter Cardiovasc Interv 2007;70:407-14.
[7] Waksman R, Pakala R, Baffour R, Seabron R, Hellinga D, Tio FO. Short-term effects of biocorrodible iron stents in porcine coronary arteries. Journal of interventional cardiology 2008;21:15-20.
[8] Peuster M, Wohlsein P, Brügmann M, Ehlerding M, Seidler K, Fink C, et al. A novel approach to temporary stenting: degradable cardiovascular stents produced from corrodible metal—results 6–18 months after implantation into New Zealand white rabbits. Heart 2001;86:563-9.
[9] Pierson D, Edick J, Tauscher A, Pokorney E, Bowen P, Gelbaugh J, et al. A simplified in vivo approach for evaluating the bioabsorbable behavior of candidate stent materials. J Biomed Mater Res B Appl Biomater 2012;100:58-67.
[10] Kirkland NT. Magnesium biomaterials: past, present and future. Corrosion Engineering, Science and Technology 2013;47:322-8.
[11] Bowen PK, Drelich J, Goldman J. Zinc exhibits ideal physiological corrosion behavior for bioabsorbable stents. Adv Mater 2013;25:2577-82.
[12] Bowen PK, Guillory RJ, 2nd, Shearier ER, Seitz JM, Drelich J, Bocks M, et al. Metallic zinc exhibits optimal biocompatibility for bioabsorbable endovascular stents. Mater Sci Eng C Mater Biol Appl 2015;56:467-72.
[13] Zberg B, Uggowitzer PJ, Loffler JF. MgZnCa glasses without clinically observable hydrogen evolution for biodegradable implants. Nat Mater 2009;8:887-91.
[14] de Jonge LT, Leeuwenburgh SC, Wolke JG, Jansen JA. Organic–inorganic surface modifications for titanium implant surfaces. Pharmaceutical research 2008;25:2357-69.
[15] Dickie RA, Floyd FL. Polymeric Materials for Corrosion Control: An Overview. 1986;322:1-16.
[16] Puskas JE, Munoz-Robledo LG, Hoerr RA, Foley J, Schmidt SP, Evancho-Chapman M, et al. Drug-eluting stent coatings. Wiley Interdiscip Rev Nanomed Nanobiotechnol 2009;1:451-62.
[17] Mathers CD, Loncar D. Projections of global mortality and burden of disease from 2002 to 2030. Plos med 2006;3:e442.
[18] Go AS, Mozaffarian D, Roger VL, Benjamin EJ, Berry JD, Blaha MJ, et al. Heart disease and stroke statistics--2014 update: a report from the American Heart Association. Circulation 2014;129:e28-e292.
[19] Nagle R. Pathophysiology of Heart Disease. Postgraduate medical journal 1988;64:910.
[20] Herzog CA, Ma JZ, Collins AJ. Comparative survival of dialysis patients in the United States after coronary angioplasty, coronary artery stenting, and coronary artery bypass surgery and impact of diabetes. Circulation 2002;106:2207-11.
[21] Investigators S. Coronary artery bypass surgery versus percutaneous coronary intervention with stent implantation in patients with multivessel coronary artery disease (the Stent or Surgery trial): a randomised controlled trial. The Lancet 2002;360:965-70.
[22] Jeewandara TM, Wise SG, Ng MK. Biocompatibility of coronary stents. Materials 2014;7:769-86.
[23] Rhee J, Sabatine M, Lilly L. Ischemic heart disease. Pathophysiology of heart disease: A collaborative project of medical students and faculty Baltimore, MD: Lippincott Williams & Wilkins 2011.
[24] Serruys PW, de Jaegere P, Kiemeneij F, Macaya C, Rutsch W, Heyndrickx G, et al. A comparison of balloon-expandable-stent implantation with balloon angioplasty in patients with coronary artery disease. New England Journal of Medicine 1994;331:489-95.

[25] Steele PM, Chesebro JH, Stanson AW, Holmes D, Dewanjee MK, Badimon L, et al. Balloon angioplasty. Natural history of the pathophysiological response to injury in a pig model. Circulation Research 1985;57:105-12.
[26] Couet F, Rajan N, Mantovani D. Macromolecular biomaterials for scaffold-based vascular tissue engineering. Macromol Biosci 2007;7:701-18.
[27] Seung KB, Park D-W, Kim Y-H, Lee S-W, Lee CW, Hong M-K, et al. Stents versus coronary-artery bypass grafting for left main coronary artery disease. New England Journal of Medicine 2008;358:1781-92.
[28] Fischman DL, Leon MB, Baim DS, Schatz RA, Savage MP, Penn I, et al. A randomized comparison of coronary-stent placement and balloon angioplasty in the treatment of coronary artery disease. Stent Restenosis Study Investigators. N Engl J Med 1994;331:496-501.
[29] Kempczinski R. Intravascular stents to prevent occlusion and restenosis after transluminal angioplasty. Journal of Vascular Surgery 1987;6:533.
[30] Gilding DK, Reed AM. Biodegradable polymers for use in surgery—polyglycolic/poly(actic acid) homo- and copolymers: 1. Polymer 1979;20:1459-64.
[31] Sigwart U, Puel J, Mirkovitch V, Joffre F, Kappenberger L. Intravascular stents to prevent occlusion and restenosis after transluminal angioplasty. N Engl J Med 1987;316:701-6.
[32] Butany J, Carmichael K, Leong SW, Collins MJ. Coronary artery stents: identification and evaluation. J Clin Pathol 2005;58:795-804.
[33] Whelan D, van Beusekom H, Krabbendam S, Ozdemir B. Eal'ly and late reactions to PLA coated and drug loaded PLA coated stents in porcine coronary arteries. Stents and Vascular Woundhealing 1999:111.
[34] Ding Y, Wen C, Hodgson P, Li Y. Effects of alloying elements on the corrosion behavior and biocompatibility of biodegradable magnesium alloys: a review. Journal of Materials Chemistry B 2014;2:1912.
[35] Jacobs JJ, Gilbert JL, Urban RM. Current concepts review-corrosion of metal orthopaedic implants. J Bone Joint Surg Am 1998;80:268-82.
[36] Ostrowski NJ, Lee B, Roy A, Ramanathan M, Kumta PN. Biodegradable poly(lactide-co-glycolide) coatings on magnesium alloys for orthopedic applications. J Mater Sci Mater Med 2013;24:85-96.
[37] Köster R, Vieluf D, Kiehn M, Sommerauer M, Kähler J, Baldus S, et al. Nickel and molybdenum contact allergies in patients with coronary in-stent restenosis. The Lancet 2000;356:1895-7.
[38] Bowen PK, Drelich J, Buxbaum RE, Rajachar RM, Goldman J. New approaches in evaluating metallic candidates for bioabsorbable stents. Emerging Materials Research 2012;1:237-55.
[39] Zheng YF, Gu XN, Witte F. Biodegradable metals. Materials Science and Engineering: R: Reports 2014;77:1-34.
[40] Peng Q, Huang Y, Zhou L, Hort N, Kainer KU. Preparation and properties of high purity Mg-Y biomaterials. Biomaterials 2010;31:398-403.
[41] Chu P, Wu G. Surface design of biodegradable magnesium alloys for biomedical applications. Surface Modification of Magnesium and its Alloys for Biomedical Applications: Biological Interactions, Mechanical Properties and Testing 2015:89.
[42] Narayanan TS, Park I-S, Lee M-H. Surface Modification of Magnesium and Its Alloys for Biomedical Applications: Biological Interactions, Mechanical Properties and Testing: Elsevier; 2015.

[43] Zeng R, Dietzel W, Witte F, Hort N, Blawert C. Progress and Challenge for Magnesium Alloys as Biomaterials. Advanced Engineering Materials 2008;10:B3-B14.
[44] Aggett P, Harries J. Current status of zinc in health and disease states. Archives of disease in childhood 1979;54:909.
[45] Hambidge KM, Krebs NF. Zinc deficiency: a special challenge. The Journal of Nutrition 2007;137:1101-5.
[46] Agrawal C, Haas K, Leopold D, Clark H. Evaluation of poly(L-lactic acid) as a material for intravascular polymeric stents. Biomaterials 1992;13:176-82.
[47] Pendyala L, Jabara R, Robinson K, Chronos N. Passive and active polymer coatings for intracoronary stents: novel devices to promote arterial healing. J Interv Cardiol 2009;22:37-48.
[48] Abizaid A, Costa JR, Jr. New drug-eluting stents: an overview on biodegradable and polymer-free next-generation stent systems. Circ Cardiovasc Interv 2010;3:384-93.
[49] Mazumder MM, De S, Trigwell S, Ali N, Mazumder MK, Mehta JL. Corrosion resistance of polyurethane-coated Nitinol cardiovascular stents. Journal of Biomaterials Science, Polymer Edition 2003;14:1351-62.
[50] Cieślik M, Engvall K, Pan J, Kotarba A. Silane–parylene coating for improving corrosion resistance of stainless steel 316L implant material. Corrosion Science 2011;53:296-301.
[51] Li JN, Cao P, Zhang XN, Zhang SX, He YH. In vitro degradation and cell attachment of a PLGA coated biodegradable Mg–6Zn based alloy. Journal of Materials Science 2010;45:6038-45.
[52] Chen Y, Song Y, Zhang S, Li J, Zhao C, Zhang X. Interaction between a high purity magnesium surface and PCL and PLA coatings during dynamic degradation. Biomed Mater 2011;6:025005.
[53] Wong HM, Yeung KW, Lam KO, Tam V, Chu PK, Luk KD, et al. A biodegradable polymer-based coating to control the performance of magnesium alloy orthopaedic implants. Biomaterials 2010;31:2084-96.
[54] Singer F, Schlesak M, Mebert C, Hohn S, Virtanen S. Corrosion Properties of Polydopamine Coatings Formed in One-Step Immersion Process on Magnesium. ACS Appl Mater Interfaces 2015;7:26758-66.
[55] Nair LS, Laurencin CT. Biodegradable polymers as biomaterials. Progress in Polymer Science 2007;32:762-98.
[56] Katarzyna Leja GL. Polymers Biodegradation and Biodegradable

Polymers – a Review. Polish J of Environ Stud 2009;19:255-66.
[57] Ulery BD, Nair LS, Laurencin CT. Biomedical Applications of Biodegradable Polymers. J Polym Sci B Polym Phys 2011;49:832-64.
[58] Xue L, Greisler HP. Biomaterials in the development and future of vascular grafts. J Vasc Surg 2003;37:472-80.
[59] Bergsma JE. A 5-year in vitro and in vivo study of the biodegradation of polylactide plates. Journal of Oral and Maxillofacial Surgery 1998;56:614-5.
[60] Commandeur S, van Beusekom HM, van der Giessen WJ. Polymers, drug release, and drug-eluting stents. J Interv Cardiol 2006;19:500-6.
[61] Tamariz E, Rios-Ramrez A. Biodegradation of Medical Purpose Polymeric Materials and Their Impact on Biocompatibility. 2013.
[62] Ali SA, Doherty PJ, Williams DF. Mechanisms of polymer degradation in implantable devices. 2. Poly(DL-lactic acid). J Biomed Mater Res 1993;27:1409-18.

[63] Kondyurin A, Kondyurina I, Bilek M. Biodegradable drug eluting coating of cardiovascular stents dewets and can cause thrombosis. arXiv preprint arXiv:11010659 2011.
[64] Venables JD. Adhesion and Durability of Metal/Polymer Bonds. 1984:453-67.
[65] Matienzo LJ, Shaffer DK, Moshier WC, Davis GD. Organic Corrosion Inhibitors to Improve the Durability of Adhesion Between Aluminum and Polymeric Coatings. 1986;322:234-49.
[66] Egitto FD, Matienzo LJ. Plasma modification of polymer surfaces for adhesion improvement. IBM Journal of Research and Development 1994;38:423-39.
[67] Bressy C, Ngo VG, Ziarelli F, Margaillan A. New insights into the adsorption of 3-(trimethoxysilyl)propylmethacrylate on hydroxylated ZnO nanopowders. Langmuir 2012;28:3290-7.
[68] Rowland SM, Stanley KD. Biocompatible metal surfaces. Google Patents; 1994.
[69] Shimp LA, Knaack D. Coupling agents for orthopedic biomaterials. Google Patents; 2007.
[70] Cahalan LL, Cahalan PT, Verhoeven M, Hendriks M, Fouache B. Biocompatible medical article and method. Google Patents; 1997.
[71] Wang Z-K, Wang D, Wang H, Yan J-J, You Y-Z, Wang Z-G. Preparation of biocompatible nanocapsules with temperature-responsive and bioreducible properties. Journal of Materials Chemistry 2011;21:15950.
[72] Liu X, Yue Z, Romeo T, Weber J, Scheuermann T, Moulton S, et al. Biofunctionalized anti-corrosive silane coatings for magnesium alloys. Acta Biomater 2013;9:8671-7.
[73] Zucchi F, Frignani A, Grassi V, Balbo A, Trabanelli G. Organo-silane coatings for AZ31 magnesium alloy corrosion protection. Materials Chemistry and Physics 2008;110:263-8.
[74] Kim J, Wong KC, Wong PC, Kulinich SA, Metson JB, Mitchell KAR. Characterization of AZ91 magnesium alloy and organosilane adsorption on its surface. Applied Surface Science 2007;253:4197-207.
[75] Zucchi F, Grassi V, Frignani A, Monticelli C, Trabanelli G. Influence of a silane treatment on the corrosion resistance of a WE43 magnesium alloy. Surface and Coatings Technology 2006;200:4136-43.
[76] Gelest I. Silane coupling agents connecting across boundries. p. 4-20.
[77] Hornberger H, Virtanen S, Boccaccini AR. Biomedical coatings on magnesium alloys - a review. Acta Biomater 2012;8:2442-55.
[78] Bowen PK, Shearier ER, Zhao S, Guillory RJ, 2nd, Zhao F, Goldman J, et al. Biodegradable Metals for Cardiovascular Stents: from Clinical Concerns to Recent Zn-Alloys. Adv Healthc Mater 2016;5:1121-40.
[79] Heldman AW, Cheng L, Jenkins GM, Heller PF, Kim DW, Ware M, et al. Paclitaxel Stent Coating Inhibits Neointimal Hyperplasia at 4 Weeks in a Porcine Model of Coronary Restenosis. Circulation 2001;103:2289-95.
[80] Fang H-W, Li K-Y, Su T-L, Yang TC-K, Chang J-S, Lin P-L, et al. Dip coating assisted polylactic acid deposition on steel surface: Film thickness affected by drag force and gravity. Materials Letters 2008;62:3739-41.
[81] Bracco G, Holst B. Surface science techniques: Springer Science & Business Media; 2013.
[82] McCafferty E. Introduction to corrosion science: Springer Science & Business Media; 2010.
[83] GAMRY INSTRUMENTS. Basics of Electrochemical Impedance Spectroscopy.
[84] Princeton Applied Research. Basics of Electrochemical Impedance Spectroscopy.
[85] Bonora PL, Deflorian F, Fedrizzi L. Electrochemical impedance spectroscopy as a tool for investigating underpaint corrosion. Electrochimica Acta 1996;41:1073-82.

[86] Hort N, Huang Y, Fechner D, Stormer M, Blawert C, Witte F, et al. Magnesium alloys as implant materials--principles of property design for Mg-RE alloys. Acta Biomater 2010;6:1714-25.
[87] Böstman O, Pihlajamäki H. Clinical biocompatibility of biodegradable orthopaedic implants for internal fixation: a review. Biomaterials 2000;21:2615-21.
[88] Yanagida H, Okada M, Masuda M, Ueki M, Narama I, Kitao S, et al. Cell adhesion and tissue response to hydroxyapatite nanocrystal-coated poly(L-lactic acid) fabric. J Biosci Bioeng 2009;108:235-43.
[89] Manninen M, Päivärinta U, Pätiälä H, Rokkanen P, Taurio R, Tamminmäki M, et al. Shear strength of cancellous bone after osteotomy fixed with absorbable self-reinforced polyglycolic acid and poly-L-lactic acid rods. Journal of Materials Science: Materials in Medicine 1992;3:245-51.
[90] Bergsma J. Late degradation tissue response to poly(L-lactide) bone plates and screws. Biomaterials 1995;16:25-31.